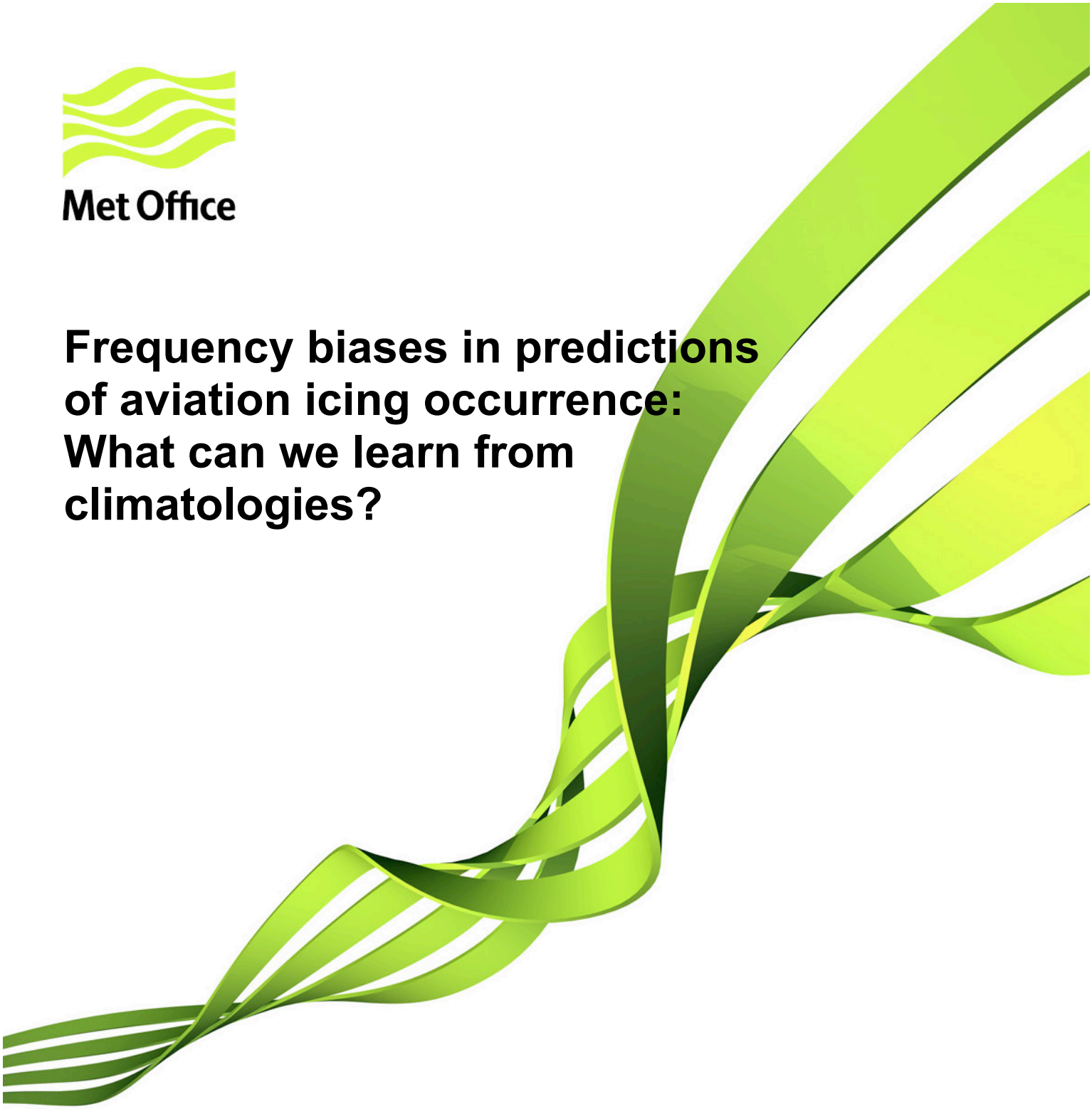

Frequency biases in predictions of aviation icing occurrence: What can we learn from climatologies?

Forecasting Research
Technical Report No: 588

22 January 2014
Cyril J. Morcrette (Met Office),
Ben C. Bernstein (Leading Edge Atmospherics, Longmont, Colorado, USA)
and Helen Wells (Met Office)

Frequency biases in predictions of aviation icing occurrence: What can we learn from climatologies?

Cyril J. Morcrette {Met Office, Exeter, UK}

Ben C. Bernstein {Leading Edge Atmospherics, Longmont, Colorado, USA} and

Helen Wells {Met Office, Exeter, UK}

Correspondence to:
Dr Cyril J. Morcrette, Met Office, FitzRoy Road, Exeter, EX1 3PB,
United Kingdom. E-mail: cyril.morcrette@metoffice.gov.uk

Abstract

The prediction of locations where aircraft are susceptible to the accumulation of ice due to the presence of supercooled liquid water is an important part of the hazard forecasts provided to aviators. We describe a method for quantitatively assessing the performance of different icing algorithms by using of model-derived climatologies and comparing them to climatologies derived from observations. This method helps identify frequency biases in potential new icing algorithms and helps in their subsequent development prior to testing in an NWP setting. Our icing-climatology evaluation method is illustrated by comparing the frequency-of-occurrence biases of a new icing algorithm to those of the index used operationally. Using the notion that the actual liquid water content (LWC) encountered by aircraft can be described using an probability density function describing the fluctuations of the LWC about the model-predicted grid-box-mean value our new index quantifies the likelihood of encountering local supercooled liquid water contents above any threshold. Our evaluation using climatologies then shows that the new index can be tuned to give unbiased predictions of icing occurrence from a climatological point-of-view. The new index is shown to capture the variations in icing frequency as a function of month, height and geographical location as well as the control icing index. However, the new index has the advantage that its formulation allows for the development of bespoke icing indices that decouple icing severity and risk. Additionally, the new index can be interpreted as a probability, allowing it to be incorporated into an ensemble-based probabilistic forecast.

© Crown copyright 2014

1 Introduction

In the Earth's atmosphere, water does not necessarily freeze as soon as it is cooled below 0°C. In the absence of abundant, active ice nuclei, water can exist as a "supercooled liquid" down to temperatures of around −40°C before homogeneous nucleation, and freezing, occurs (e.g. Rogers and Yau, 1989). In natural clouds however, supercooled water is most commonly found at temperatures close to 0°C and less frequently as temperatures decrease. Using data from a lidar onboard the space shuttle, Hogan *et al.* (2004) estimated that, in the latitude range ±60°, there was liquid water present in around 20% of the clouds whose temperature was between −10°C and −15°C and that this proportion dropped to essentially zero for clouds with temperatures colder than −35°C.

When water is in a supercooled liquid state, the introduction of ice nuclei may lead to the rapid freezing of the liquid onto the nuclei and then onto the newly formed ice mass. Airplanes, helicopters and other objects such as power lines, antennae and wind turbines can also act as the surface onto which supercooled liquid water freezes. The build-up of ice on an aircraft's structure is known as "aircraft icing" or simply "icing". The accumulation of ice on an aircraft's wings, propellers, fuselage or external flight instruments can have a negative impact on its manoeuvrability and performance with potentially catastrophic consequences (e.g. Politovich, 2003; Cole and Sand, 1991; Lankford, 2001).

Since aircraft icing is due to the presence of supercooled liquid water in the atmosphere, then meteorologically, the problem becomes one of predicting the existence of clouds in the right temperature range, then differentiating between those clouds that are likely to be dominated by supercooled liquid, rather than ice. Automated icing forecasts are typically produced taking temperature and humidity information from a numerical weather prediction (NWP) model. As a result the quality of the icing forecast is very dependent on the realism of the temperature and humidity which the model predicts will prevail at a particular time and place (Thompson *et al.*, 1997).

Bernstein *et al.* (2005) reviewed different icing diagnosis and forecasting techniques. Some methods, based purely on NWP model temperature and humidity, without including information about the cloud cover and liquid water content, tended to overpredict the occurrence of icing and would sometimes predict icing in regions which were actually cloud-free. To mitigate this issue, Tafferner *et al.* (2003), Le Bot (2004) and Bernstein *et al.* (2005) developed icing indices that combined temperature and humidity information from short-lead-time NWP forecasts with cloud observations from satellite and reflectivity information from ground-based radar. These algorithms all employed a scenario-based approach, while Bernstein *et al.* (2005) also used fuzzy logic membership functions to capture some of the inherent uncertainty and variability in both icing probability and severity. McDonough *et al.* (2004) and Wolff *et al.* (2009) extended this approach to develop forecasts of icing out to 18 hours.

It is common to evaluate icing forecasts using aircraft observations of icing, such as pilot reports (PIREPS), since these are a strong, fairly direct indication of the phenomenon being forecast (Brown *et al.*, 1997). There are issues with using PIREPS however. Firstly, PIREPS of icing conditions exhibit spatial and temporal patterns that are artifacts of air-traffic density and the daily and weekly pattern in the number of flights that occur (Schultz and Politovich, 1992). Secondly, PIREPS of "no icing" are under-represented because pilots are more likely to report the presence of

© Crown copyright 2014

icing rather than its absence. Although it is possible to infer the absence of icing conditions from some of the other information contained in the PIREPS, any statistical evaluation of icing algorithms must be done with careful consideration of these sampling biases (Brown *et al.*, 1997). Finally, PIREPS do not provide an easy means of assessing the severity of an icing forecast. This is because the PIREPS of icing severity are subjective in nature and represent a combination of the meteorological environment, the aircraft type, the ice protection system, how it is applied, flight history and pilot perception (Sand and Biter, 1997).

Morcrette *et al.* (2012) discussed the evaluation of cloud cover forecasts and the different types of cloud forecast errors. Their conclusions can also be applied to the evaluation of icing forecasts and so Fig. 1 shows a Venn diagram illustrating the different ways in which an icing forecast can be in error. When assessing the statistical performance of an icing forecast over a long period, the forecast can be incorrect due to an error in: i) frequency of occurrence (FOO) of icing conditions, ii) amount when present (AWP, i.e. the severity of icing when icing is predicted) and iii) timing. As an example of the different aspects of the icing forecast error, an icing forecast could over-predict the FOO of generic icing conditions, but under-predict the AWP, or severity, leading to the FOO of severe icing conditions actually appearing to be quite accurate. Averaged over a long period, an icing index could also correctly predict the FOO and the severity in a mean sense, but get the timing wrong, for example, by consistently predicting icing too early or late in the day.

When assessing the skill of a large number of icing predictions statistically all three error components will be present (as illustrated by the white region in the centre of the Venn diagram). In order to improve the performance of an icing prediction system, one needs to think about the sources of the errors. Inaccuracies in icing predictions can be due to a variety of causes, as shown around the perimeter of Fig. 1. An icing prediction can turn out to be wrong because of errors in the model's microphysics, the model's grid-resolved condensate amount and fractional cloud cover or the icing algorithm. It can also be wrong due to errors in the large-scale thermodynamic state, either because of errors in the model evolution or due to the analysis used to initialise the forecast. The severity of an icing risk can also appear wrong due to issues to do with defining severity and the degree to which icing severity is influenced by aeronautical as well as meteorological factors.

One reason for measuring the skill of any forecast is to compare the relative performance of two systems. This helps when developing new forecasting methods as it enables a comparison with the current operational system. Quantitative measures of relative performance can also be used when deciding to replace an operational product with a newly-developed one.

This paper argues that it is important to know which aspects of the icing forecast error a particular evaluation method is sensitive to. Additionally, one should aim to have an icing-forecast evaluation method that measures these different aspects of the icing forecast errors. This is because certain measures of skill are very sensitive to one aspect of the error. If one only considers a single skill metric, one can get a misleading picture of the relative performance of two forecasting systems. If one makes improvements to the aircraft icing algorithm, in order to tackle one aspect of the forecast error but only assesses it using a metric that is very sensitive to another aspect of the error, which has not changed, then one can be misled as to whether the changes made to the algorithm have actually improved anything. Icing forecasts can be evaluated using the Equitable Threat Score (ETS or Gilbert Skill Score, Gilbert (1884)) which quantify the skill with which observed events were forecast. However this skill score is very sensitive to timing errors and the double penalty effect. This is

© Crown copyright 2014

aside from the fact that the Equitable Threat Score turns out not to be equitable (Hogan *et al.*, 2010).

Since icing indices tend to be so dependent on the model's prediction of temperature and humidity (Thompson *et al.*, 1997) then if there is a timing error in the model's large-scale flow, for example due to problems with the model's initial conditions, or due to the incorrect evolution of the atmosphere caused by problems with the model's physical parametrization schemes, then that error will still be present no matter how the icing forecast algorithm is re-formulated. As a result comparing the relative performance of two icing algorithms by using the ETS will not be particularly informative.

So out of the three aspects of the icing forecast error: timing, severity and frequency of occurrence, it seems that evaluating the frequency of occurrence may be the most helpful from the point of view of developing and testing potential new aircraft icing indices.

Bernstein *et al.* (2007) and Bernstein and Le Bot (2009) describe climatologies of icing conditions inferred from several years' worth of surface weather reports, balloon soundings and model re-analyses. These icing climatologies estimate the frequency of occurrence of icing conditions geographically and as a function of height and month of the year for 15 sites around the world (Fig. 2). The patterns found in these studies compared favourably with large independent datasets of observed icing from PIREPs over the U.S. and surface observations from mountain sites in Europe.

The Met Office has a seamless forecasting system (Brown *et al.*, 2012), which means that there is a general circulation model (GCM) configuration which can be used for operational global NWP and that the same model and choice of parametrization schemes can be used to perform global climate simulations. This configuration is known as Global Atmosphere 3.0 (GA3.0, Walters *et al.*, 2011). In this study, a multi-year simulation of the present-day climate will be used as input to a variety of icing algorithms. This will enable us to determine the frequency of icing conditions at the 15 locations documented in the climatologies as predicted by each algorithm. The various icing algorithms will then be assessed in terms of their ability to reproduce the site-to-site, monthly and altitude variations of the inferred icing climatologies derived from indirect observations. The various icing algorithms will be assessed specifically in terms of the error in their frequency of occurrence (see Fig. 1). That is to say, the icing algorithms will be evaluated in terms of their ability to predict the frequency of occurrence of the inferred icing climatologies derived from indirect observations, including their ability to reproduce the site-to-site, monthly and altitude variations. Although we do not suggest that a new icing algorithm can be verified solely by using a climatology, we believe that the evaluation of the model-predicted icing climatology is an important step in assessing the performance of any new icing algorithms.

One of the important features of GA3.0 compared to the previous global operational NWP model configuration is the inclusion of the prognostic cloud, prognostic condensate, cloud scheme (PC2, Wilson *et al.*, 2008a). This scheme has been shown to lead to an improved representation of cloud in both the climate (Wilson *et al.*, 2008b) and weather forecasting context (Morcrette *et al.*, 2012). The PC2 cloud scheme has 5 prognostic variables: liquid and frozen condensate and liquid, frozen and total cloud fraction. Due to the presence of mixed-phase regions, the total cloud fraction is not necessarily equal to the sum of the liquid and frozen cloud fractions.

© Crown copyright 2014

The PC2 scheme calculates sources and sinks for each of these prognostics variables and advects the updated cloud variables using the model winds. Each of the following physical processes can modify the cloud fields: short-wave radiation, long-wave radiation, boundary-layer mixing, precipitation formation (microphysics), sub-grid-scale convective motions, sub-grid-scale mixing (erosion) and grid-resolved ascent and adiabatic cooling (Wilson *et al.*, 2008a). The microphysics scheme in the MetUM (Wilson and Ballard, 1999; Walters *et al.*, 2011) considers a number of physical processes including homogeneous and heterogeneous freezing, depositional growth, fall, melting and sublimation of ice. It also includes autoconversion and accretion of liquid water to rain and riming of liquid, capture of raindrops by ice and evaporation of rain.

Following Morcrette and Petch (2010), Fig. 3 uses annual-mean global cloud-scheme process rates to show the relative contribution of each parametrized physical process to the sources (Fig. 3a) and sinks (Fig. 3b) of liquid water content and to the sources (Fig. 3c) and sinks (Fig. 3d) of liquid cloud fraction. The PC2 cloud scheme represents the impact of all these physical processes that can create and remove cloud and is designed to represent all cloud types: from large-scale cloudiness associated with synoptic-scale ascent, to the partial cloudiness, and relatively high in-cloud water contents, associated with convective regimes. Using data from the quantitative studies of Morcrette and Petch (2010) and Morcrette (2012b), Fig. 4 provides a schematic of the dominant cloud source and sink terms that are acting in different cloud regimes. In the mid-latitudes, the convection scheme is a source of cloud in the cold sector of extra-tropical cyclones and along the cold front. Large-scale ascent is also important along both the cold and warm fronts. Boundary-layer mixing is an important cloud-formation process in the warm sector. The formation of precipitation within the cloud, and the cloud erosion associated with the mixing of clear and cloudy air at cloud edges, are the main sink terms for liquid cloud. When considering a cross-section from sub-tropical stratocumulus to tropical deep convection one finds that the stratocumulus cloud decks are replenished by long-wave cooling from cloud top and boundary-layer mixing. These source processes are offset by cloud erosion and the microphysical transfer of cloud water to precipitation which then falls out of the cloud. As the boundary-layer and long-wave cooling sources diminish, the cloud regime often transitions to broken shallow convective clouds where the convection scheme becomes a key source term. In the tropics, the dominant cloud creation process is convection, which is balanced by sinks from microphysics and cloud erosion.

As one of only two World Area Forecasting Centres (WAFC), the Met Office (referred to as WAFC-London) provides forecasts of the risk of en-route icing conditions for use by aviation. The use of the new PC2 cloud scheme in the operational global forecast model is the perfect opportunity to revisit the icing algorithm currently being used and to ask whether a better forecast algorithm could be developed that makes use of the improved temperature, cloud and humidity fields produced by the new model configuration and which could be incorporated into an ensemble-based probabilistic forecasting system. The first step in our icing index development strategy is to consider how a new icing index might be evaluated. This paper describes a method for evaluating the frequency of occurrence characteristics of proposed new icing indices. This is demonstrated by developing and testing a series of hypothetical new icing indices and showing that, from a statistical point of view, some of them can perform as well as the current operational (control) algorithm.

The current WAFC-London icing algorithm is reviewed in Section 2 before describing a series of potential new indices of increasing complexity. In section 3 we present a method for the statistical evaluation of proposed icing indices from a climatological

© Crown copyright 2014

point-of-view and illustrate its use by showing that one of these new indices, which has a much better scientific basis, can perform as well as the current index, when assessed against the climatologies. Section 4 provides a discussion. A summary and conclusions are given in Section 5.

2 Description of icing indices (II)

2.1 Some existing icing indices

Several icing indices (II) are considered in this paper and are listed in Table 2 in order of increasing complexity. In each case the algorithm starts by assigning the II a default value of zero to each location in space and time. Then, using data from an NWP forecast, the algorithm considers each model grid-box at each output time and checks whether the temperature is in the range of 0 to −20°C. If it is, the numerical value of the II is set based on information about the local humidity or cloud. Finally, the algorithm checks whether the II is above a critical value, ii_{crit}. If it is, then the algorithm is predicting an icing risk. The critical value can be different for each II, reflecting the statistical properties of each, which depend on how it is defined.

One method of calculating an II is the “Class I” algorithm described by Schultz and Politovich (1992). For those points whose temperature is between 0 to -20°C, the icing index is set equal to the relative humidity (RH). This II based on RH is referred to as II(RH) in Table 2. The icing index currently used in the Met Office/WAFC-London products is similar to the “Class I” algorithm of Schultz and Politovich (1992). For grid-points in the right temperature range, the algorithm checks if the three-dimensional cloud fraction field is greater than zero. If there is cloud present, the three-dimensional icing index is set to the RH. This index, based on RH if cloud is present, will henceforth be referred to as II(RHCldPres).

2.2 Some other icing indices

One feature of II(RH) and II(RHCldPres) is that they are both dimensionless and typically have a value between 0.0 and around 1.0. In practice however, the lower limit of II(RHCldPres) is determined by the critical RH required for cloud to form in the model. This critical RH is usually between 0.8 and 0.95 and is generally specified, or calculated, as part of the fractional cloud cover parametrization scheme. As a result of II(RH) and II(RHCldPres) being dimensionless and typically having values between 0.0 and 1.0 they have sometimes been interpreted as a probability. However, this is not how these indices should be used. This is because there is no reason why the grid-box-mean RH should directly quantify the chance of encountering icing conditions within a grid-box. Additionally, although large supersaturation with respect to liquid is rare in the atmosphere, RH values greater than 1.0 do have a physical meaning. An II based on RH could in principle report values greater than 1.0, but these would make no sense if the II is interpreted as a probability. In practice, the II(RHCldPres) is capped at 1.0, within the icing algorithm code, prior to being disseminated to WAFC-London for use in producing the icing forecast.

General circulation models used for global NWP make use of cloud parametrization schemes to determine the fraction of the model grid-box which is covered by cloud based on information about the local thermodynamic state (e.g. Smith, 1990) and, increasingly, using information about the other physical processes occurring at the same location (e.g. Tiedtke, 1993; Tompkins, 2002; Wilson *et al.*, 2008a; Watanabe *et al.*, 2009).

© Crown copyright 2014

In the next sub-section, a proposed new icing index is described. This will make use of information about both the grid-box fractional cloud cover and the grid-box-mean liquid water content. However, before describing the relatively complex index which uses both of these inputs, it seems sensible to check whether the same inputs could be used directly to develop a simpler icing index.

The model grid-box's cloud fraction (CF), that is the fraction of the grid-box which is covered by cloud, is an intuitive choice as an input for a potential new II. This will be referred to as II(CF) and we note that in this case the algorithm is using the generic cloud fraction, which means it is not distinguishing between condensed water in the liquid or ice phase. In the MetUM, the liquid cloud fraction (LCF) is available as a separate variable. This allows us to consider a slightly different index, II(LCF), which is based on the fraction of the grid-box containing condensate in the liquid phase.

One feature of the PC2 cloud scheme is the relative independence with which the LCF and liquid water content (LWC) can vary. Although the existence of non-zero LCF must imply non-zero LWC and vice-versa, the PC2 scheme is able to produce a wide range of LWC for a given LCF (Wilson *et al.*, 2008b). As a result, it is reasonable to consider whether using grid-box-mean LWC as an input would produce a significantly different new II. This will be called II(LWC), where the LWC is in gm^{-3} rather than kg kg^{-1}.

For the purposes of developing icing indices, it is useful to consider the minimum supercooled LWC, q_T, which poses a risk to aviation. Although this minimum value will vary depending on the aircraft and also depends on the presence of supercooled large drops, which are not considered here, a value of $q_T = 0.1 gm^{-3}$ seems a sensible threshold and is consistent with the values reported by Politovich (2003) and with those used in the wind-tunnel studies of Ide (1999).

To aid comparison with the other II, II(LWC) is normalised by dividing by $2q_T$. This means that II(LWC) will be dimensionless and will have a value of 0.5 if the grid-box-mean LWC, q_{cl}, is equal to the threshold LWC, q_T.

The grid-box-mean LWC, q_{cl}, is the value of LWC that one would obtain if the condensed water was distributed evenly across the grid-box. As we have seen however, the model also predicts the LCF, C_l, so a more sensible variable for use in an icing index is the mean LWC within the clouds, that is the in-cloud LWC (icLWC), which is defined as q_{cl}/C_l. This index, which is also normalised by dividing by $2q_T$, will be called II(icLWC).

Even within the cloudy portion of a grid-box however, there is considerable variability in the amount of condensate. The importance of this variability on the clouds' radiative impact (Cahalan *et al.*, 1994) has led to the development of radiation schemes, such as the Monte Carlo Independent Column Approximation (McICA), which sample this variability (Pincus *et al.*, 2003). From the point of view of forecasting icing conditions, the variability in sub-grid-scale supercooled LWC is likely to be very important. Indeed, just because the mean in-cloud LWC is below a given threshold does not mean that the threshold is not exceeded anywhere within the grid-box.

By assuming that the sub-grid cloud variability can be described by an analytic function, Räisänen *et al.* (2004) generated a sample of sub-grid-scale cloudy conditions, consistent with the grid-box-mean cloud cover, condensate amount and some information about the standard deviation of the condensate. These were then used when performing radiation calculations.

© Crown copyright 2014

In the next sub-section, we use similar ideas about the sub-grid-scale variability in LWC to develop a new icing index that quantifies the probability of encountering supercooled LWC above a certain threshold somewhere within the model grid-box.

2.3 A proposed new icing index

Figure 5 shows some photographs of clouds containing supercooled liquid water. In an NWP model, these cloud fields could typically be represented by only a single grid-box in the horizontal. This grid-box would have a single value of fractional cloud cover, C_l, and a single grid-box mean liquid water content, q_{cl}. There is variability in the real cloud field however and some parts of the clouds may have a high enough liquid water content that they pose a risk to aviation while some parts will have much lower liquid water content. Some portion of the grid-box may be altogether cloud-free.

To demonstrate the use of climatologies in evaluating potential new icing indices, we have developed a new icing index which aims to estimate the fraction of the model grid-box that contains local liquid water content, q_{cl}, above a certain threshold, q_T. Following Räisänen *et al.* (2004), we assume that within the cloudy part of the grid-box, the variability in the local water content, q_{cl}, can be described by an analytical probability density function (PDF), which we will call $P(q_{cl})$. The mean value of this PDF is set to the mean in-cloud LWC, calculated by dividing the grid-box mean LWC, q_{cl}, by the liquid cloud fraction, C_l. Later, it will also be necessary to specify the fractional standard deviation of the sub-grid variability. This PDF is then integrated between the limits of the threshold LWC, q_T, and infinity, using some analytical solutions. This integral will give, F, the fraction of the cloudy region with LWC above the threshold. The fraction of the sky with LWC above the threshold, or the chance (χ) of encountering local LWC above the threshold, is then found by multiplying this integral, F , by the grid-box-mean liquid cloud fraction, C_l:

$$\chi(q_\tau) = F(q_\tau)C_l = C_l \int_{q_\tau}^{\infty} P(q_{cl})dq_{cl}$$

Equation 1

The concept behind the χ icing index is illustrated in Fig. 6 using a gamma PDF, a mean in-cloud water content of $q_{cl}/C_l = 5.0 \times 10^{-5}$ kg kg^{-1} and a fractional standard deviation, $f_c = 0.75$. The threshold LWC is 1.0×10^{-4} kg kg^{-1} and the portion of the PDF where the local LWC is greater than the threshold, around 10% in this case, is shaded in Fig. 6a. It is worth noting that although the mean is half the threshold value, while the mode is smaller still, a part of the cloud is expected to have local LWC above the threshold value because of the PDF's long tail. An example of the variability in local LWC across a model grid-box with a cloud cover of $C_l = 0.5$ is shown in Fig. 6b. In this example, there are 200 samples, which are randomly determined to be cloudy or clear, and if cloudy their LWC is taken from the gamma PDF. Despite, the cloud only covering 50% of the grid-box and the mean in-cloud water content being half of the threshold value, around 5% of the grid-box has a local LWC higher than the threshold. This is a non-negligible amount. It is this aspect of sub-grid variability in LWC and its link to aircraft icing that we wish to build into our new algorithm.

The rest of this subsection describes the functional form of the LWC PDF, documents the parametrization of the standard deviation that will be used in calculating it and explains the numerical techniques used for integrating Equation 1.

© Crown copyright 2014

2.3.1 Justification for using analytical PDF

Ground-based remote-sensing observations of liquid water cloud are used to infer the sub-grid-scale variability in LWC. The observations were made at the Atmospheric Radiation Measurement (ARM, Stokes and Schwartz, 1994) or Cloud-Net (Illingworth *et al.*, 2007) sites at Chilbolton, Darwin, Lindenberg, Murgtal and the Southern Great Plains (Oklahoma) during the month of April 2007 as described in (Morcrette *et al.*, 2012). The observed LWC were averaged onto the MetUM grid in the vertical. The observations were also averaged in time, using the model wind-speed, for the time it would take a cloud to be advected the length of the grid-box. This time-averaging creates a horizontal sample comparable to the size of the GCM grid-boxes used in the simulations described in Section 3.

In order to compare the PDF of LWC from grid-boxes with a large variation in grid-box mean LWC, the individual LWC observations have been normalised by the corresponding grid-box mean LWC before calculating the PDF. Figure 7 shows the observed PDF of LWC within a grid-box, alongside a gamma and log-normal PDF which have the same mean and standard deviation as the observed PDF. Both analytical PDFs are a fair representation of the observed distribution, although both produce a mode smaller than the mean, which is not seen in the observations. The gamma distribution, however, is better at capturing the probability of the mode.

Using a gamma PDF within an icing algorithm has the advantage that conceptually the assumptions about sub-grid variability would then be consistent with the cloud-generator which is used by McICA and which have been included into the MetUM radiation parametrization scheme (Hill *et al.*, 2011). For completeness, however, we include the description of the icing index derived using both the gamma and log-normal PDF assumptions and compare both of them to the observed climatology.

2.3.2 Gamma distribution

The variability in LWC within the cloudy part of the grid-box can be defined by a gamma distribution given by:

$$P(x) = \frac{1}{\Gamma(k)\theta^k} x^{k-1} e^{-x/\theta}$$

Equation 2

where k and θ are the shape and scale parameters respectively. The mean, m, and variance, v, of the variable x are given by

$$m = k\theta$$

Equation 3

and

$$v = k\theta^2$$

Equation 4

which can be re-arranged to give θ and k in terms of m and v:

$$\theta = v/m$$

Equation 5

and

© Crown copyright 2014

$$k = m/\theta$$

Equation 6

2.3.3 Log-normal distribution

Alternatively, the in-cloud LWC variability can be represented using a log-normal distribution given by:

$$P(x) = \frac{1}{x\sqrt{2\pi\sigma^2}} e^{-\frac{(\ln(x)-\mu)^2}{2\sigma^2}}$$

Equation 7

where μ and σ are the mean and standard deviation of the logarithm of the variable x. The mean, m, and variance, v, of the variable x are given by

$$m = e^{\mu+\frac{\sigma^2}{2}}$$

Equation 8

and

$$v = \left(e^{\sigma^2} - 1\right)e^{2\mu+\sigma^2}$$

Equation 9

which can be re-arranged to give μ and σ in terms of m and v:

$$\mu = \ln(m) - \frac{1}{2}\ln\left(\frac{v}{e^{2\ln(m)}} + 1\right)$$

Equation 10

and

$$\sigma = \sqrt{2\ln(m) - 2\mu}$$

Equation 11

2.3.4 Closing the LWC PDF parametrization

Since we are considering the PDF of in-cloud LWC, the mean value of the PDF, m, is set equal to the mean in-cloud LWC derived from the grid-box mean LWC, q_{cl}, and grid-box mean liquid cloud fraction, C_l:

$$m = \frac{\overline{q_{cl}}}{C_l}$$

Equation 12

Now the variance, v, of the PDF, is the square of its standard deviation, s. Additionally, the fractional standard deviation of the condensate, f_c, is defined as the standard deviation, s, divided by the mean, m, so

$$v = s^2 = (mf_c)^2$$

Equation 13

In order to complete the parametrization of the sub-grid-scale LWC variability we need to specify the fractional standard deviation, f_c, of the PDF.

Following on from the work of Hill *et al.* (2012), remote-sensing data collected by Cloud-Sat, Cloud-Net/ARM and in-situ observations made by atmospheric-research

© Crown copyright 2014

aircraft were used by Boutle *et al.* (2013) to derive a parametrization for the fractional standard deviation of LWC as a function of grid-box size and cloud cover. This parametrization takes the form of:

$$f_c = \begin{cases} (0.54 - 0.25C_l)\phi_c(x, C_l) & C_l < 1 \\ 0.11\phi_c(x, C_l) & C_l = 1 \end{cases}$$

Equation 14

where

$$\phi(x, C_l) = (xC_l)^{1/3}\left((0.06xC_l)^{1.5} + 1\right)^{-0.17}$$

Equation 15

and x is the size of the grid-box in kilometres. The variation of f_c as a function of cloud fraction and grid-box size is illustrated in Fig. 8. The Boutle *et al.* (2013) parametrization of f_c is used here to close the gamma and log-normal PDFs for use in two new icing algorithms called II(χ-Γ) and II(χ-LN), respectively.

2.3.5 Fraction of cloud with LWC above threshold

Having specified a LWC PDF, $P(q_{cl})$, the fraction of cloud, F, with a local LWC above a certain threshold q_τ is:

$$F = \int_{q_\tau}^{\infty} P(q_{cl})dq_{cl} = 1 - CDF(q_\tau)$$

Equation 16

where CDF is the Cumulative Density Function given by:

$$CDF(q_\tau) = \int_0^{q_\tau} P(q_{cl})dq_{cl}$$

Equation 17

For a gamma distribution, the CDF is given by

$$CDF(q_\tau) = \frac{1}{\Gamma(k)}\gamma\left(k, \frac{q_\tau}{\theta}\right)$$

Equation 18

where $\gamma(k, q_\tau/\theta)$ is calculated from the lower incomplete gamma function, defined as

$$\gamma(s, x) = x^s\Gamma(s)e^{-x}\sum_{n=0}^{\infty}\frac{x^n}{(s+n+1)}$$

Equation 19

In the icing algorithm, this is calculated by doing the summation up to n = 20. An example of a gamma distribution and its associated F = 1−CDF is shown in Fig. 9. Alternatively, if the PDF is defined by using a log-normal distribution then the CDF is given by:

$$CDF = \frac{1}{2} + \frac{1}{2}erf\left(\frac{\ln(q_\tau) - \mu}{\sqrt{2\sigma^2}}\right)$$

Equation 20

where erf is the error function defined as:

© Crown copyright 2014

$$erf(x) = \frac{2}{\sqrt{\pi}} \int_0^x e^{-t^2} dt$$

Equation 21

Using Taylor expansion this can be written as:

$$erf(x) = \frac{2}{\sqrt{\pi}} \sum_{n=0}^{\infty} \frac{(-1)^n z^{2n+1}}{n!(2n+1)}$$

Equation 22

In the icing algorithm this is implemented by expanding up to the 13th order:

$$erf(x) = \frac{2}{\sqrt{\pi}} \left(x - \frac{x^3}{3} + \frac{x^5}{10} - \frac{x^7}{42} + \frac{x^9}{216} - \frac{x^{11}}{1320} + \frac{x^{13}}{9360} \right)$$

Equation 23

An example of a log-normal distribution and its associated F = 1−CDF is also shown in Fig. 9.

The variation in F = 1−CDF as a function of liquid cloud fraction and liquid water content for a sub-grid variability defined using a gamma and log-normal PDF is shown in Fig. 10(a and b). In both cases the fractional standard deviation, f_c, is assumed to be 0.75. Multiplying by the liquid cloud fraction gives χ which is shown in Fig. 10(c and d).

Throughout this paper, χ is calculated using a threshold of $q_T = 1.0 \times 10^{-4}$ kg kg^{-1} . If a different threshold were to be used, we propose that the term χ-LN or χ-Γ should be followed by the q_T threshold used in calculating it, i.e. χ-Γ(1.0×10^{-4}).

3 Calibration of model-derived icing indices using observed climatology

3.1 Method

The icing indices listed in Table 2 and described in Section 2 will be assessed by comparing their climatologies as a function of location, height and time of the year against some climatologies inferred from observations. Bernstein *et al.* (2007) and Bernstein and Le Bot (2009) produced month-height plots of the frequency of icing conditions aloft at 15 sites world-wide. The data from these two climatologies are shown in Fig. 2 while the locations of each of the sites are given in Table 1.

It is worth noting that the vertical axes in Fig. 2 are with respect to sea-level. The altitude of each site is given in Table 1 and is indicated by the thin black line across the bottom of each panel. In many cases, the site is near enough to sea-level that the black line is not discernibly higher than the x-axis. At Guiyang, which is 1074 m above sea-level, the absence of an icing occurrence below 1 km simply reflects the altitude of the site. Similarly, Denver, with an altitude of 1655 m, does not have any icing occurrence below 1 km. The icing that occurs between 1 and 2 km above sea-level must however all actually be occurring between 1655 and 2000m, that is between 0 and 345 m above ground level.

For this study, the MetUM has been run as an atmosphere-only climate model, forced by observed sea-surface temperatures. The simulation starts on 1 Sept 1981 and runs for 20 years and 3 months. The first 3 months are then discarded to allow for spin-up.

© Crown copyright 2014

A detailed description of the package of atmospheric parametrizations used in the GA3.0 configuration is given by Walters *et al.* (2011). For our purposes, we note that the model uses the PC2 cloud scheme (Wilson *et al.*, 2008a,b). The model is run using the L85 vertical grid, which has 85 vertical levels, 50 of which are below 18km and the model top is at a height of 85 km. The horizontal resolution is N96, leading to a regular latitude-longitude grid of 145 × 192 points. For the 15 sites being considered the mean grid-box dimension is around 138 km.

At each of the 15 sites that appear in the climatologies of Bernstein *et al.* (2007) and Bernstein and Le Bot (2009), profiles of temperature, humidity, pressure, density, liquid cloud fraction, generic cloud fraction and liquid cloud condensate are output from the model. These are output every 20 minute timestep for the entirety of the 20 year run. The information from all of these thermodynamic profiles is then used to calculate what each of the 8 icing indices in Table 2 would predict at that place, time and height.

Then for each site, we go through the 20 years and check whether the icing index is above a certain threshold. If it is, the icing index is assumed to have "predicted icing conditions". We then calculate the frequency of predicted icing conditions for each height and month, by looking at the entire 20-year period. This analysis considers 11 thresholds in turn: 0.01, 0.02, 0.05, 0.10, 0.20, 0.40, 0.60, 0.80, 0.90, 0.95, 0.98 and the procedure is repeated for each of the 8 icing indices.

3.2 Results

Figure 11 shows profiles of frequency of icing conditions for each of the icing indices and each of the thresholds. The profile of observed frequency of icing conditions, averaged over all the sites and months is shown for comparison. The first thing to note is that although all the icing indices produce values between 0 and 1, the distribution of values produced by each index is very different. As a result, the value of the icing index above which the index should be interpreted as having predicted icing conditions will be different for each index. Consequently, if one replaces one index by another within an operational system, the threshold value will also need to be changed.

As an example the current icing index, II(RHCldPres), reproduces the observed profile of icing conditions the best when using a critical value of around 0.95 (magenta) and over-predicts the occurrence of icing when using a threshold below that (Fig. 11b). The index based on generic cloud fraction, II(CF), matches the observed climatological frequency of icing occurrence quite well when using a threshold of 0.6 (blue, Fig. 11c) however this leads to an overprediction at heights below 2 km. II(LCF) and II(LWC) both match the observed profile above 3 km quite well when using a critical value of around 0.1 (green) although they then overpredict icing occurrence below that height (Fig. 11d and e). The two version sof the χ index give very similar results, as is to be expected since the only difference between them is whether the sub-grid-cloud variability is represented using a log-normal or gamma PDF.

The two icing indices based on χ also both capture the shape of the icing frequency profile above 3 km when using a critical value of 0.02 (orange), however they also both over-predict the frequency of icing conditions below 3 km. This over-prediction in the frequency of occurrence of icing conditions at lower levels is consistent with the over-prediction of the frequency of occurrence of low and mid-level liquid cloud identified by Morcrette *et al.* (2012) when comparing predictions of cloud cover using

© Crown copyright 2014

GA3.0 to observations from ARM and Cloud-Net sites. Consequently, the over-prediction of icing conditions exhibited by the χ indices is not thought to be a deficiency of the χ algorithm, but rather, it is related to a cloud bias seen in the host model. Future developments of the GA configuration, such as changing the formulation of liquid cloud erosion (Morcrette, 2012a), may improve this bias.

We now investigate the ability of each of the icing indices to reproduce the observed climatologies in terms of the variation in frequency of occurrence of icing as a function of location, height and month. For each icing index, we consider the time-height climatologies shown in Fig. 2, and calculate the bias and root-mean-squared error (RMSE) between the frequency of occurrence predicted by each index and the frequency of occurrence inferred from the observations. This comparison is done using icing index thresholds ranging from 0.01 to 0.99 in steps of 0.01 and is repeated for each of the icing indices (Fig. 12).

The control icing index II(RHCldPres) has zero bias when using an ii_{crit} value of around 0.96. II(CF) has zero bias when using a critical value of around 0.62, while values of 0.10, 0.12 and 0.80 lead to unbiased frequency of occurrence using II(LCF), II(LWC) and II(icLWC), respectively. The χ-LN and χ-Γ indices have no bias when using ii_{crit} values of around 0.06. The ability of the icing algorithms to reproduce the observed climatology can also be quantified by looking at the RMSE in the frequency of occurrence, hence quantifying the ability of the indices to predict the correct variation of icing frequency with height and month of the year. All the indices tend to have lower RMSE as their biases are reduced, however the critical value which leads to the lowest bias does not lead to the lowest RMSE and vice versa (Fig. 12). Interestingly, the magnitude of the smallest RMSE that can be achieved by each index is very similar. Additionally, the RMSE associated with an unbiased χ prediction is comparable to the RMSE associated with an unbiased prediction using the control algorithm, II(RHCldPres). So by using an appropriate value of ii_{crit} , the χ indices can perform as well as the operational control index from the point of view of long-term statistics.

For each icing index, we can then find the ii_{crit} values which lead to unbiased prediction of icing frequency when compared to climatology when assessed over all the sites, months and heights. Figure 13 shows the time-height plots of icing frequency predicted by the control icing index, II(RHCldPres), when using an ii_{crit} of 0.96 to determine that icing conditions are likely. Figure 14 shows the time-height plots using the new χ-Γ algorithm and an ii_{crit} of 0.06. The climatology produced using the II(χ-LN) algorithm, and a critical value of 0.06, is very similar to the one produced using II(χ-Γ) using the same critical value (not shown). The fact that the overall frequency of occurrence for both model-derived climatologies is comparable to the observed climatology simply reflects the fact that, in this analysis, the model-derived indices have been calibrated against the observational data. However, this is the first time that a potential icing algorithm for use in NWP has been calibrated in this way and it may prove to be a useful part of the icing index development process.

Visual comparison of the model-predicted icing climatologies (Figs. 13 and 14) with the observed climatology (Fig. 2) shows that the two icing index climatologies computed from climate model output are capable of reproducing the broad features of the variability of icing frequency as a function of height, month and geographical location.

As before, we note that the vertical axes in Figs. 13 and 14 are with respect to sea-level. The height of the model orography at the locations used in the climatology does not necessarily match the height of the true orography. This is due to the desire

© Crown copyright 2014

to avoid orographic forcing near the grid-scale, which can compromise the stability of the numerical model. As a result, the orography is smoothed, however this is not a trivial exercise as one wishes to maintain the height of important mountain ridges, while preventing sea points from being raised above sea-level (e.g. Rutt et al., 2006). The height of the model orography at the model grid-point nearest to each of the sites is indicated by the thin black line across the bottom of each panel in Figs. 13 and 14. In most cases, the model orography and true orography are within 200 m of each other. One notable exception is Denver. Since it is only 25 km east of the edge of the Rocky Mountains the nearest grid point has a height of 2446 m, nearly 800 m higher than the true orography. As a result, the lowest altitude above sea-level the 140 km grid-length model can predict the occurrence of icing at Denver is 2446 m. This explains the absence of predicted icing between 1 and 2 km in Figs. 13e and 14e.

4 Discussion

Closer comparison between Figs. 2, 13 and 14 reveals a number of interesting results. The II(RHCldPres) algorithm fails to predict any icing occurrence in July or August over Flint, Michigan, despite its existence having been inferred from the observations. The II(χ-Γ) algorithm does predict some icing over Flint during the summer, however its occurrence is over too shallow a layer (4-6 km compared to 3-7 km).

Neither of the II do a particularly good job of predicting the summer-time occurrence of icing over Denver. This is probably due to the model failing to initiate enough convective storms in the lee of the Colorado Front Range as a result of not accurately resolving the details of the flow associated with the shape of the orography. Due to its simplicity, the II(RHCldPres) algorithm performs slightly better over Denver as it only relies of the presence of some cloud and high RH, rather than high in-cloud LWC, as is the case for II(χ). The under-estimation of icing frequency over Sofia in summer, which is also located close to steep orography, is presumably due to a similar issue concerning the initiation of convective storms. Looking at the icing frequency predicted at Trappes (Paris), the II(RHCldPres) produces a peak in the frequency of occurrence in December and January between 1 and 2 km, while the observations suggest a deeper maximum that extends over several months. The new χ index is better at capturing this longer-lasting increase in the frequency of icing occurrence through the autumn and winter months. In the climatologies inferred from the observations, Wajima and Tateno, on the western and eastern sides of Japan, exhibit a noticeably different frequency of icing conditions during the winter months of December, January and February. For the climatologies produced by the model however, the data for the two locations look more similar to each other, irrespective of
whether II(RHCldPres) or II(χ) is used. This is again likely to be due to the relatively coarse horizontal resolution and the smoothed orography which prevents the model from accurately representing the flow near the Japanese Alps and its impact on the local meteorology. Looking at the other sites, it seems that the χ algorithm tends to under-estimate the height up to which icing occurs. This is less evident for II(RHCldPres). This suggests that it is not the absence of cloud, nor the temperature range that is preventing χ from predicting the occurrence of icing conditions at higher levels, but rather the fact that the clouds in the model may have glaciated and that the condensed water in the clouds is in the solid rather than liquid phase. This issue with the χ algorithm could be addressed by revisiting the microphysical process rate involved in the freezing of liquid to ice. Due to the implications that this would have on the distribution of latent heating, the hydrological cycle and the radiative balance

© Crown copyright 2014

of the model, this is beyond the scope of this paper, however it will be considered as part of the future evaluation of II(χ) in an NWP setting.

One issue with three-dimensional (3D) data, such as the χ indices discussed here, is how best to present the 3D data as a two-dimensional (2D) field, for example for displaying on a map. One option is to consider a range of flight levels (e.g. 0 to 3,000 ft) and to search for the maximum value of the icing index within that height range. The same notion can be used, when considering the whole atmospheric column, to give the maximum icing index that occurs in the column. This maximum value, either within a height range or within the whole column, can then be plotted as contours on a map.

Another way of producing a 2D total column icing index is to use the notion of maximum/random overlap (MRO) that is commonly used when considering clouds and radiation in the atmosphere (Geleyn and Hollingsworth, 1979; Räisänen, 1998). When considering cloud cover on a number of separate model levels, the MRO algorithm assumes maximum overlap between vertically continuous cloud layers but random overlap when any cloud layers are separated by some clear sky. If the icing conditions occurring at different heights do not have any clear sky between them, then the MRO algorithm will just give the maximum value of the icing index. However, if the vertical distribution of icing conditions is convex at any point in the profile, then the MRO algorithm will report a higher value than the simple maximum; hence accounting for the fact that all the icing conditions are not expected to all be perfectly aligned in the vertical. In principle, the MRO algorithm can be applied over a finite depth or over the entire atmospheric column. By applying the MRO algorithm over the entire depth of the 3D χ indices, we obtain a 2D field, which we call "MRO-χ". This can be intepreted as the probability of encountering icing conditions as one flies from the surface to cruising altitude (or vice versa) while traversing a significant portion of the horizontal dimension of the grid box, as an aircraft would do during take-off or landing. Multi-year means of MRO-χ are shown for 4 different months throughout the annual cycle in Fig. 15. Overall, the maps of MRO-χ produce similar spatial patterns and seasonal variations as the maps of icing frequencies in Fig. 12 of Bernstein and Le Bot (2009).

Figure 15 shows that apart from in boreal summer, there are relatively few occurrences of icing predicted through-out the polar regions. This is due to the 0 to −20°C temperature range used in the calculation of the icing index and the fact that the model only has relatively few clouds warmer then −20°C at these high latitudes. In July by contrast, the model predicts the existence of clouds warmer than −20°C and lots of icing is predicted through-out the Arctic. This seasonal increase is not seen in Antarctica, presumably as the higher elevation means that supercooled liquid water clouds are less common than in the north. All months show an increase in the frequency of icing occurrence located in the mid-latitude storm tracks as well as a smaller maximum in the inter-tropical convergence zone. Simulations using a higher resolution model would be expected to better represent the structures of the tropical and extra-tropical systems within which these supercooled liquid clouds occur, hence leading to a better prediction of the location of icing conditions. This is an area for future work.

5 Summary and Conclusions

As we develop new algorithms that use NWP model output to predict the risk of icing to aviation, there is the need to quantitatively assess whether one algorithm is better

© Crown copyright 2014

than another. However, the error in an icing forecast can take on different forms. An icing algorithm can give an incorrect forecast either because it predicts the wrong frequency of occurrence of icing conditions, or because it has predicted the wrong severity, or because it has got the timing or exact location of the event wrong. One way of quantitatively comparing icing algorithms is to consider individual forecast and observed events, populate a contingency table of hits, misses, false-alarms and correct negatives and calculate a variety of skill scores. This approach however is very sensitive to timing and location errors and the double-penalty effect.

In this paper we presented a method for evaluating the frequency-of-occurrence behaviour of different icing indices by comparing the icing predictions produced by a multi-year atmospheric-model simulation against a climatology of icing occurrence inferred from observations. This allowed us to evaluate the ability of different icing indices to reproduce the variation of icing occurrence as a function of location, month and height. We believe that this kind of quantitative information about climatological-mean performance can be very useful prior to running detailed icing-prediction case-studies in an NWP context.

Our icing-climatology evaluation method was illustrated by assessing a number of increasingly complex icing algorithms building on the rather simple one currently used operationally. Although the model-produced predictions of icing occurrence are not perfect, they are certainly encouraging, especially since the model was running with a relatively coarse horizontal resolution of around 140 km. Indeed, we showed that from the point-of-view of an icing-occurrence climatology our new χ index, which quantifies the chance of encountering local supercooled liquid water content above a certain threshold, performs as well as the control icing index.

One aspect of the χ algorithm is that it relies on the model correctly predicting the phase of the condensate. However, it may be that the phase of the condensate is not always correct in the model, for example, because the microphysics scheme is too efficient at converting liquid to ice. As the model's microphysics scheme is developed and improved, this is likely to directly feed in to improvements to the χ indices, although it will be necessary to revisit the values of ii_{crit}. It may also be worth considering the possible benefits of lowering the value of −20°C used in defining the temperature range over which the algorithms calculate the icing indices. Future work should also involve a comparison between the model-predicted icing indices and in-situ aircraft observations of supercooled liquid water.

We have shown, that one of the advantages of the two χ algorithms is that they have a better physical basis than the relative humidity-based icing indices. This is because the χ indices aim to predict the fraction of a given region that is likely to contain amounts of supercooled liquid water contents above a value that is deemed to be a threat to aircraft.

The second advantage of the formulation of the χ algorithms is that they can provide icing indices that clearly, and separately, account for both icing severity and risk. The χ icing index is likely to be of use to decision-makers involved in the operation of a broad range of airplanes, helicopters and wind turbines. The threshold LWC, q_T, which was here set to 1.0×10^{-4} kg kg^{-1}, can be modified to any value, based on information provided by the end-user. Information from the decision-makers, including their tolerance to false alarms and misses, can also be used when deciding on the critical value of the index above which it is deemed that there is an icing risk. The χ algorithms described here, combined with information about the end-users' susceptibility to supercooled LWC and cost-loss ratio, would allow the development

© Crown copyright 2014

of bespoke icing indices which are physically meaningful, mathematically traceable and best suited to their needs.

Finally, the χ algorithms have the important advantage that they predict a probability of encountering significant amounts of supercooled LWC. As such, they are perfectly suited to incorporating into an ensemble-based probabilistic forecasting system and this is an area of active research.

Acknowledgements

Thanks are due to Jon Petch and Roy Kershaw for comments relating to an earlier version of this document and to Greg Thompson for his encouragement during a very useful discussion. Concerning the data used in Fig. 7, the observations from Darwin, Murgtal and the Southern Great Plains were obtained from the Atmospheric Radiation Measurement (ARM) Program, funded by U. S. Department of Energy; the observations from Chilbolton were obtained by the Chilbolton Facility for Atmospheric and Radio Research, which is mainly funded by the U.K. Natural Environment Research Council and the observations from Lindenberg were obtained by the Lindenberg Meteorological Observatory, which is operated by Deutscher Wetterdienst, Germany's National Meteorological Service.

References

Bernstein, B., McDonough, F., Politovich, M., Brown, B., Ratvasky, T., Miller, D., Wolff, C., and Cunning, G. (2005). Current icing potential (CIP): Algorithm description and comparison with aircraft observations. J. Appl. Meteor., 44, 118132.

Bernstein, B. C. and Le Bot, C. (2009). An inferred climatology of icing conditions aloft, including supercooled large drops. Part II: Europe, Asia and the Globe. J. Appl. Meteor. Climatol., 48, 1503–1526.

Bernstein, B. C., Wolff, C. A., and McDonough, F. (2007). An inferred climatology of icing conditions aloft, including supercooled large drops. Part I: Canada and Continental United States. J. Appl. Meteor. Climatol., 46, 1857–1878.

Boutle, I. A., Abel, S. J., Hill, P. G., and Morcrette, C. J. (2013). Spatial variability of liquid cloud and rain: observations and microphysical effects. Q. J. Roy. Meteor. Soc., ?, ? DOI: 10.1002/qj.2140.

Brown, A., Milton, S., Cullen, M., Golding, B., Mitchell, J., and Shelly, A. (2012). Unified modeling and prediction of weather and climate: a 25 year journey. B. Am. Meteorol. Soc., 93, 1865–1877. DOI:10.1175/BAMS-D-12-00018.1.

Brown, B. G., Thompson, G., Buintjes, R. T., Bullock, R., and Kane, T. (1997). Intercomparison of in-flight icing algorithms. Part II: Statistical verification results. Weather and Forecasting, 12, 890–914.

Cahalan, R. F., Ridgway, W., Wiscombe, W. J., Bell, T. L., and Snider, J. B. (1994). The albedo of fractal stratocumulus clouds. J. Atmos. Sci., 51, 2434–2455.

Cole, J. and Sand, W. (1991). Statistical study of aircraft icing accidents. Proc. 29th Aerospace Sci. Mtg. Reno, Nevada, Amer. Inst. Aero. Astro., Washington D.C., AIAA 91-0558.

© Crown copyright 2014

Geleyn, J.-F. and Hollingsworth, A. (1979). An economical analytical nethod for the computation of the interaction between scattering and line absorption if radiation. Beitr. Phys. Atmos., 52, 1–16.

Gilbert, G. F. (1884). Finley's tornado predictions. Amer. Meteor. J., 1, 166–172.

Hill, P. G., Manners, J., and Petch, J. C. (2011). Reducing noise associated with the Monte Carlo Independent Column Approximation for weather forecasting models. Q. J. Roy. Meteor. Soc., 137, 219–228. DOI:10.1002/qj.732.

Hill, P. G., Hogan, R. J., Manners, J., and Petch, J. C. (2012). Parametrizing the horizontal inhomogeneity of ice water content using CloudSat data products. Q. J. Roy. Meteor. Soc., tba, tba. DOI: 10.1002/qj.1893.

Hogan, R. J., Ferro, C. A. T., Jolliffe, I. T., and Stephenson, D. B. (2010). Equitability revisited: Why the Equitable Threat Score is not equitable. Weather and Forecasting, 25, 710–726.

Hogan, R. J. H., Behera, M. D., OConnor, E. J., and Illingworth, A. J. (2004). Estimate of the global distribution of stratiform supercooled liquid water clouds using the LITE lidar. Geophysical Research Letters, 31(L05106). doi:10.1029/2003GL018977.

Ide, R. F. (1999). Comparison of liquid water content measurement techniques in an icing wind tunnel. Technical Report ARL-TR-2134 / NASA/TM-1999-209643, U. S. Army Research Laboratory / NASA, Glenn Research Centre, Cleveland, Ohio.

Illingworth, A. J., Hogan, R. J., O'Connor, E. J., Bouniol, D., Brooks, M. E., Delanoe, J., Donovan, D. P., Eastment, J. D., Gaussiat, N., Goddard, J. W. F., Haeffelin, M., Baltink, H. K., Krasnov, O. A., Pelon, J., Piriou, J.-M., Protat, A., Russchenberg, H. W. J., Seifert, A., Tompkins, A. M., van Zadelhoff, G.-J., Vinit, F., Willen, U., Wilson, D. R., and Wrench, C. L. (2007). CloudNet - continuous evaluation of cloud profiles in seven operational models using ground-based observations. B. Am. Meteorol. Soc., 88, 883–898.

Lankford, T. T. L. (2001). Aviation Weather Handbook. McGraw-Hill, London. ISBN: 0-07-136103-0.

Le Bot, C. (2004). SIGMA: System of icing geographic identification in meteorology for aviation. In Preprints, 11th Conf. on Aviation Range and Aerospace Meteorology, Hyannis, MA, page P6.5. Amer. Meteorol. Soc. https://ams.confex.com/ams/pdfpapers/81704.pdf.

McDonough, F., Bernstein, B. C., Politovich, M. K., and Wolff, C. A. (2004). The forecast icing potential algorithm. In 42nd Aerospace Sciences Meeting and Exhibit. American Institute of Aeronautics and Astronautics. AIAA 2004-0231, http://arc.aiaa.org/doi/abs/10.2514/6.2004-231.

Morcrette, C. J. (2012a). Improvements to a prognostic cloud scheme through changes to its cloud erosion parametrization. Atmos. Sci. Let., 13, 95–102. DOI: 10.1002/asl.374.

Morcrette, C. J. (2012b). Prognostic-cloud-scheme increment diagnostics: a novel addition to the case-study tool kit. Atmos. Sci. Let., 13, 200207. DOI: 10.1002/asl.380.

© Crown copyright 2014

Morcrette, C. J. and Petch, J. C. (2010). Analysis of prognostic cloud scheme increments in a climate model. Q. J. Roy. Meteor. Soc., 136, 2061–2073. DOI: 10.1002/qj.720.

Morcrette, C. J., O'Connor, E. J., and Petch, J. C. (2012). Evaluation of two cloud parametrization schemes using ARM and Cloud-Net observations. Q. J. Roy. Meteor. Soc., 138, 964–979. DOI:10.1002/qj.969.

Pincus, R., Barker, H. W., and Morcrette, J.-J. (2003). A fast, flexible, approximate technique for computing radiative transfer in inhomogeneous cloud fields. J. Geophys. Res., 108(D13). DOI:10.1029/2002JD003322.

Politovich, M. K. (2003). Aircraft icing. In J. R. Holton, J. A. Curry, and J. A. Pyle, editors, Encyclopedia of atmospheric science, pages 68–75. Academic Press. ISBN 0-12-227090-8.

Räisänen, P. (1998). Effective longwave cloud fraction and maximum-random overlap of clouds: A problem and a solution. Mon. Weather Rev., 126, 3336–3340.

Räisänen, P., Barker, H. W., Khairoutdinov, M. F., Li, J., and Randall, D. A. (2004). Stochastic generation of subgrid-scale cloudy columns for large-scale models. Q. J. Roy. Meteor. Soc., 130, 2047–2067.

Rogers, R. R. and Yau, M. K. (1989). A Short Course in Cloud Physics. Butterworth-Heinemann, 225 Wildwood Avenue, Woburn, MA 01801-2041, 3 edition.

Rutt, I. C., Thuburn, J., and Staniforth, A. (2006). A variational method for orographic filtering in NWP and climate models. Q. J. Roy. Meteor. Soc., 132, 17951813. DOI:10.1256/qj.05.133.

Sand, W. R. and Biter, C. (1997). Pilot response to icing: It depends. In Preprints, Seventh Conf. on Aviation, Range, and Aerospace Meteorology, Long Beach, CA, pages 116–119. Amer. Meteor. Soc.

Schultz, P. and Politovich, M. K. (1992). Towards the improvement of aircraft-icing forecasts for the Continental United States. Weather and Forecasting, 7, 491–500.

Smith, R. N. B. (1990). A scheme for predicting layer cloud and their water content in a general circulation model. Q. J. Roy. Meteor. Soc., 116, 435–460.

Stokes, G. M. and Schwartz, S. E. (1994). The Atmospheric Radiation Measurement (ARM) program: programmatic background and design of the cloud and radiation test bed. B. Am. Meteorol. Soc., 75, 1201–1221.

Tafferner, A., Hauf, T., Leifeld, C., Hafner, T., Leykauf, H., and Voigt, U. (2003). ADWICE: Advanced diagnosis and warning system for aircraft icing environments. Weather and Forecasting, 18, 184–203.

Thompson, G., Buintjes, R. T., Brown, B. G., and Hage, F. (1997). Intercomparison of in-flight icing algorithms. Part I: WISP94 real-time icing prediction and evaluation program. Weather and Forecasting, 12, 878–889.

Tiedtke, M. (1993). Representation of clouds in large-scale models. Mon. Weather Rev., 121, 3040–3061.

© Crown copyright 2014

Tompkins, A. (2002). A prognostic parameterization for the subgrid-scale variability of water vapor and clouds in large-scale models and its use to diagnose cloud cover. J. Atmos. Sci., 59, 1917–1942.

Walters, D. N., Best, M. J., Bushell, A. C., Copsey, D., Edwards, J. M., Falloon, P. D., Harris, C. M., Lock, A. P., Manners, J. C., Morcrette, C. J., Roberts, M. J., Stratton, R. A., Webster, S., Wilkinson, J. M., R., W. M., Boutle, I. A., Earnshaw, P. D., Hill, P. G., MacLachlan, C., Martin, G. M., Moufouma-Okia, W., Palmer, M. D., Petch, J. C., Rooney, G. G., Scaife, A. A., and Williams, K. D. (2011). The Met Office Unified Model Global Atmosphere 3.0/3.1 and JULES Global Land 3.0/3.1 configurations. Geosci. Model Dev., 4, 919–941. DOI:10.5194/gmd-4-919-2011.

Watanabe, M., Emori, S., Satoh, M., and Miura, H. (2009). A pdf-based hybrid prognostic cloud scheme for general circulation model. Clim. Dynam., 33, 795–816. DOI:10.1007/s00382-008-0489-0.

Wilson, D. R. and Ballard, S. P. (1999). A microphysically based precipitation scheme for the UK Meteorological Office Unified Model. Q. J. Roy. Meteor. Soc., 125, 1607–1636.

Wilson, D. R., Bushell, A. C., Kerr-Munslow, A. M., Price, J. D., and Morcrette, C. J. (2008a). PC2: A prognostic cloud fraction and condensation scheme. I: Scheme description. Q. J. Roy. Meteor. Soc., 134, 2093–2107.

Wilson, D. R., Bushell, A. C., Kerr-Munslow, A. M., Price, J. D., Morcrette, C. J., and Bodas-Salcedo, A. (2008b). PC2: A prognostic cloud fraction and condensation scheme. II: Climate model simulations. Q. J. Roy. Meteor. Soc., 134, 2109–2125.

Wolff, C., McDonough, F., Politovich, M. K., and Cunning, G. (2009). The forecast icing product: Recent upgrades and improvements. In 1st AIAA Atmospheric and Space Environments Conference. American Institute of Aeronautics and Astronautics. AIAA 2009-3531, http://arc.aiaa.org/doi/abs/10.2514/6.2009-3531.

© Crown copyright 2014

Name	Lat (°N)	Lon (°E)	Alt (m)
Resolute Bay, Canada	74.7	-94.9	66
Flint, Michigan, USA	43.0	-83.7	238
Caribou, Maine, USA	46.9	-68.0	191
Quillayute, Washington, USA	47.9	-124.5	59
Denver, Colorado, USA	39.7	-105.0	1655
Trappes (Paris), France	48.8	2.0	168
Rome, Italy	41.8	12.2	3
Sofia, Bulgaria	42.8	23.4	595
Belfast, Northern Ireland	54.5	-6.1	5
Keflavik, Iceland	64.0	-22.6	54
Oslo, Norway	60.2	11.1	204
Taipei City, Taiwan	25.0	121.5	8
Guiyang, China	26.4	106.5	1074
Wajima, Japan	37.4	136.9	14
Tateno, Japan	36.0	140.1	31

Table 1: Name, latitude, longitude and altitude of sites in Bernstein et al. (2007) and Bernstein and Le Bot (2009) climatologies.

No.	Short Name	Description
1	II(RH)	Relative humidity.
2	II(RHCldPres)	Relative humidity if cloud is present.
3	II(CF)	Cloud fraction (condensate in either liquid or ice phase).
4	II(LCF)	Liquid Cloud fraction (condensate in liquid phase).
5	II(LWC)	Grid-box mean liquid water content (normalised by threshold LWC value).
6	II(icLWC)	In-cloud liquid water content (normalised by threshold LWC value).
7	II(χ-LN)	Chance of encountering local LWC above threshold using a log-normal PDF.
8	II(χ-Γ)	Chance of encountering local LWC above threshold using a Γ PDF.

Table 2: Summary of the 8 Icing Indices (II) that are discussed in the text, including the abbreviations used and a brief description of each one.

© Crown copyright 2014

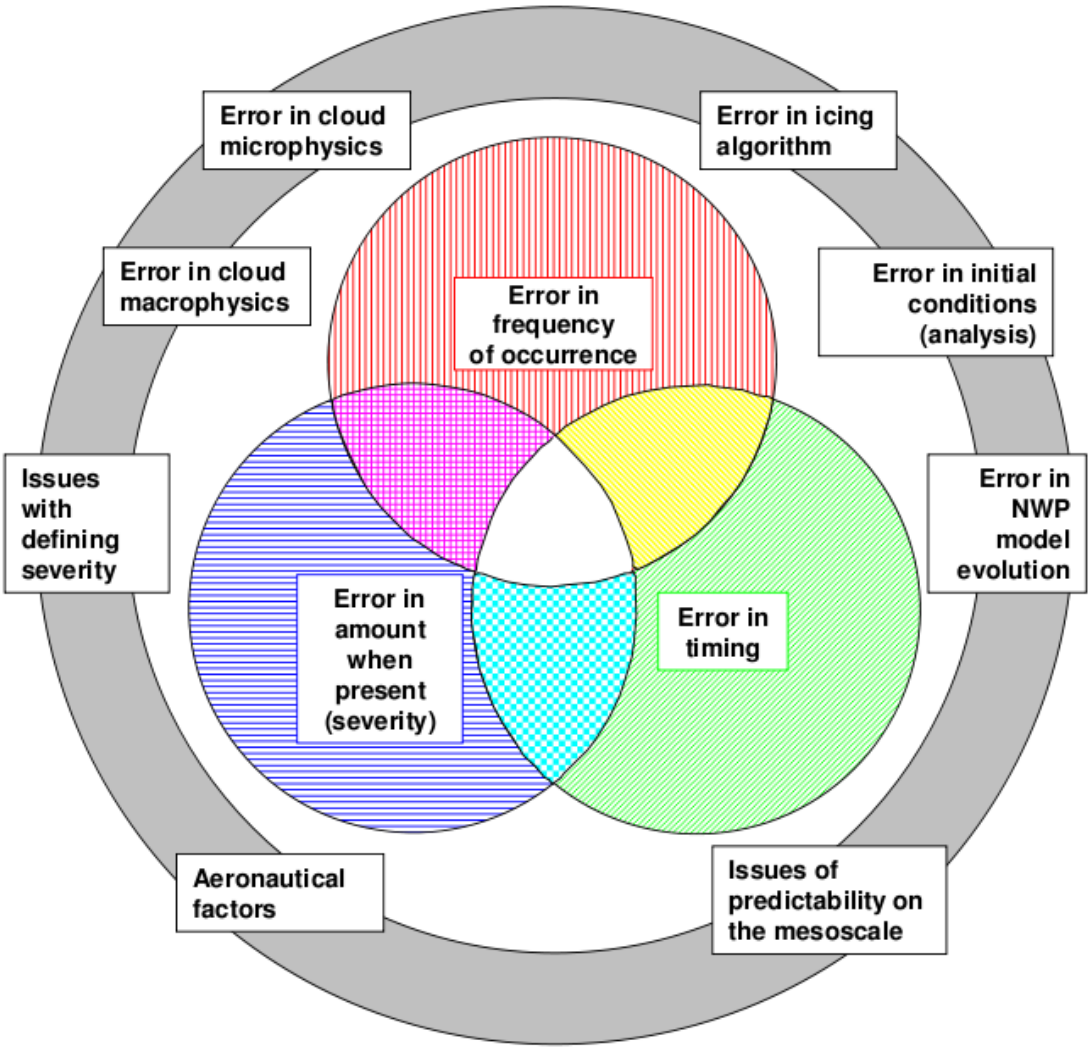

Figure 1: Venn diagram illustrating the ways in which an aviation-icing forecast can be wrong when assessed over a long period. The icing product can have an error in i) the frequency of occurrence of icing conditions, ii) the timing of the icing events and iii) the severity of the events. When assessing any icing prediction system, all three types of errors will be present. Additionally the errors will be due to a variety of causes, some examples of which are given around the edge of the diagram.

© Crown copyright 2014

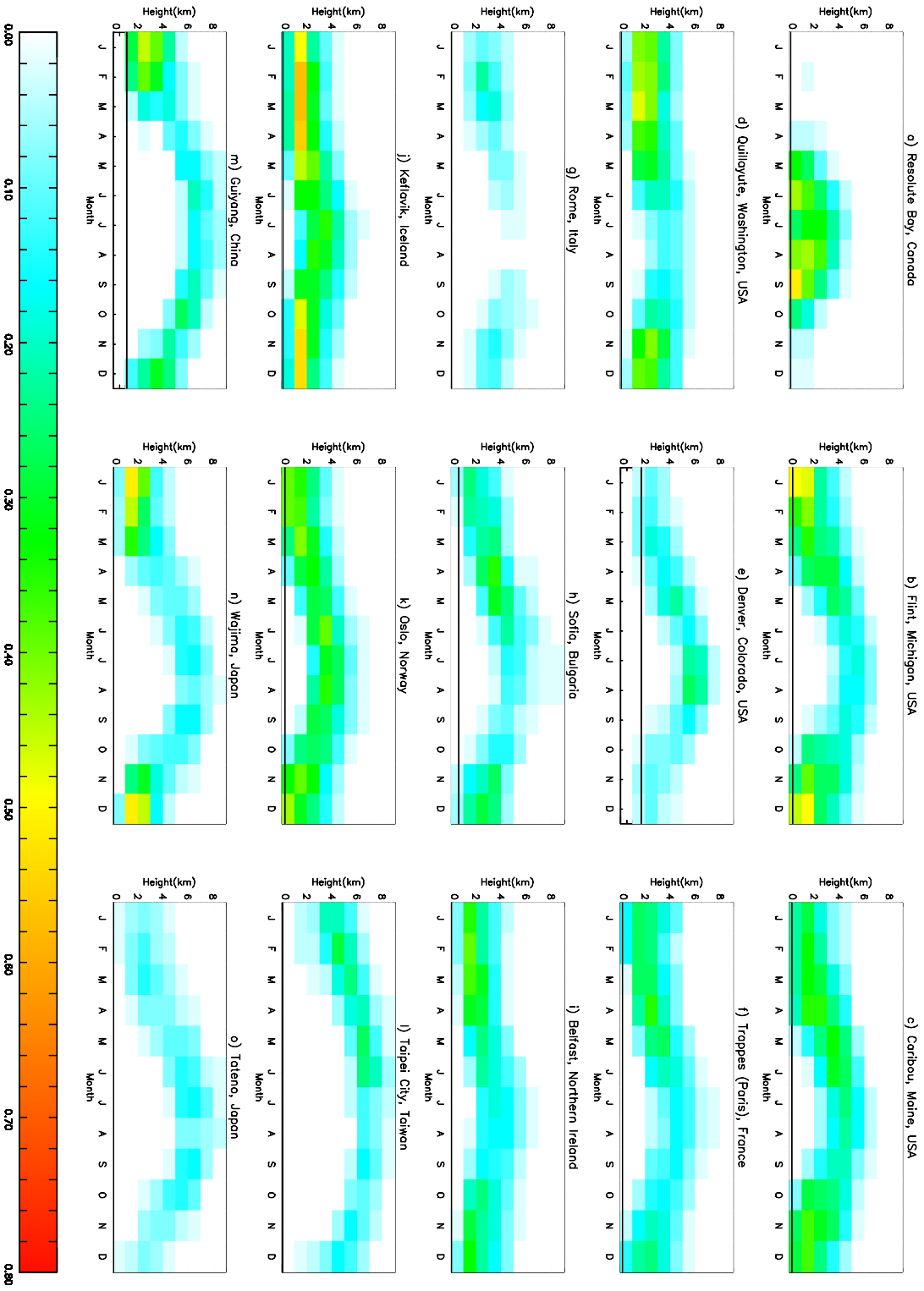

Figure 2: Time-height plots of frequency of occurrence of icing conditions at 15 sites world-wide (replotted from Bernstein et al. (2007) and Bernstein and Le Bot (2009)). The thin black line across the bottom of each panel indicates the altitude of each site. The location of the 15 sites are given in Table 1.

© Crown copyright 2014

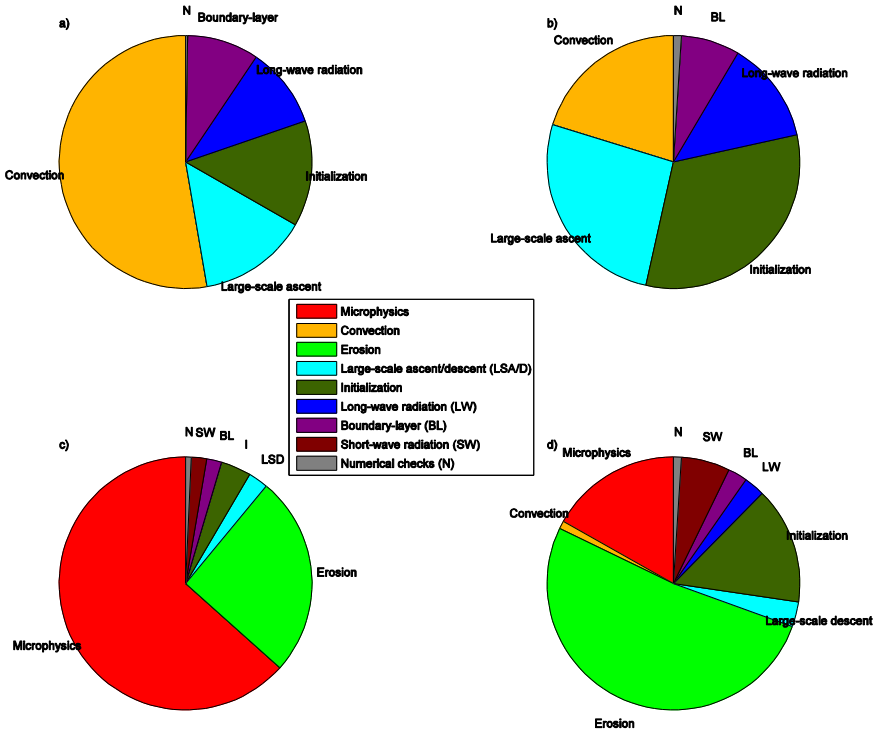

Figure 3: Pie charts showing the relative contribution of each parametrized atmospheric process to the creation (a and b) and removal (c and d) of liquid water content (a and c) and liquid cloud fraction (b and d).

© Crown copyright 2014

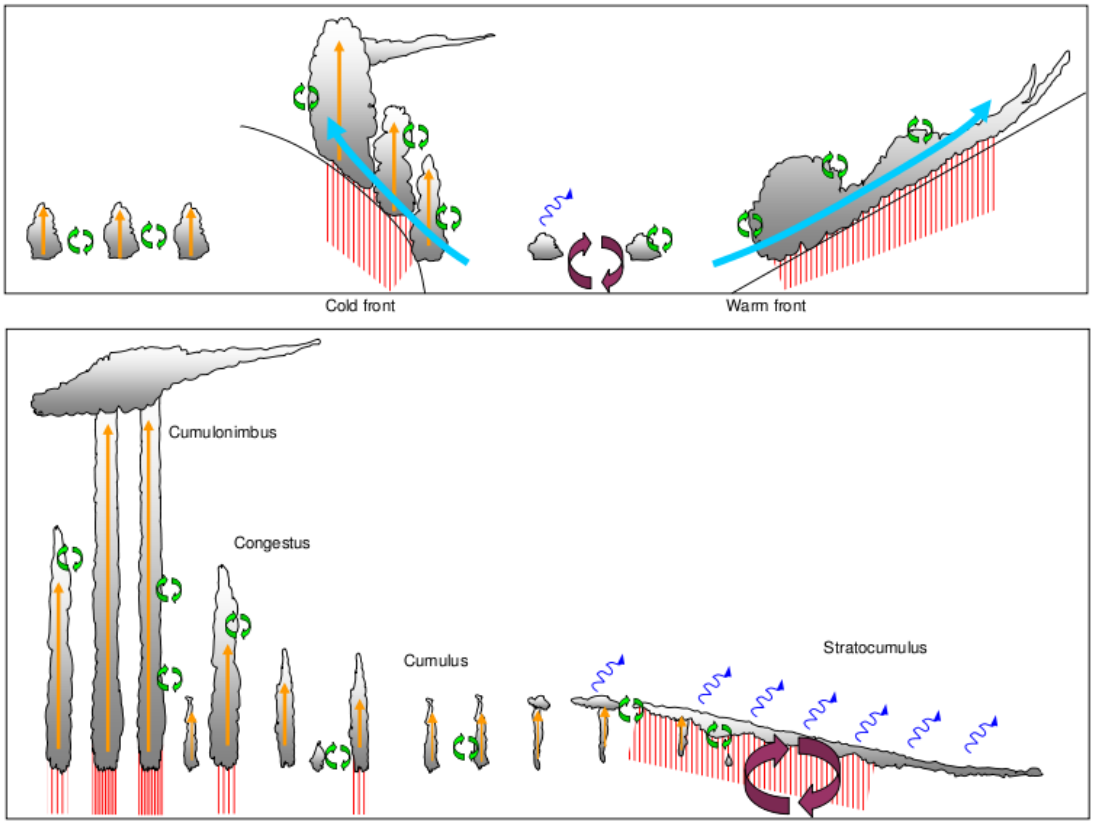

Figure 4: Schematic of the dominant parametrized physical processes contributing to the creation and removal of cloud cover and condensate in a model using the PC2 cloud scheme; a) from left to right, a cross-section through a mid-latitude cold sector, cold front, warm sector and warm front and b) from right to left, a cross-section from the sub-tropical stratocumulus regime, through the stratocumulus-to-cumulus transition and into the tropical deep convective regime. The colour of the symbols, which matches the colours used in Fig. 3, correspond to: orange = convection, cyan = large-scale ascent, purple = boundary-layer mixing, blue = long-wave radiation, green
= erosion, red = microphysics.

© Crown copyright 2014

Figure 5: Photographs of clouds containing liquid water below 0°C.

© Crown copyright 2014

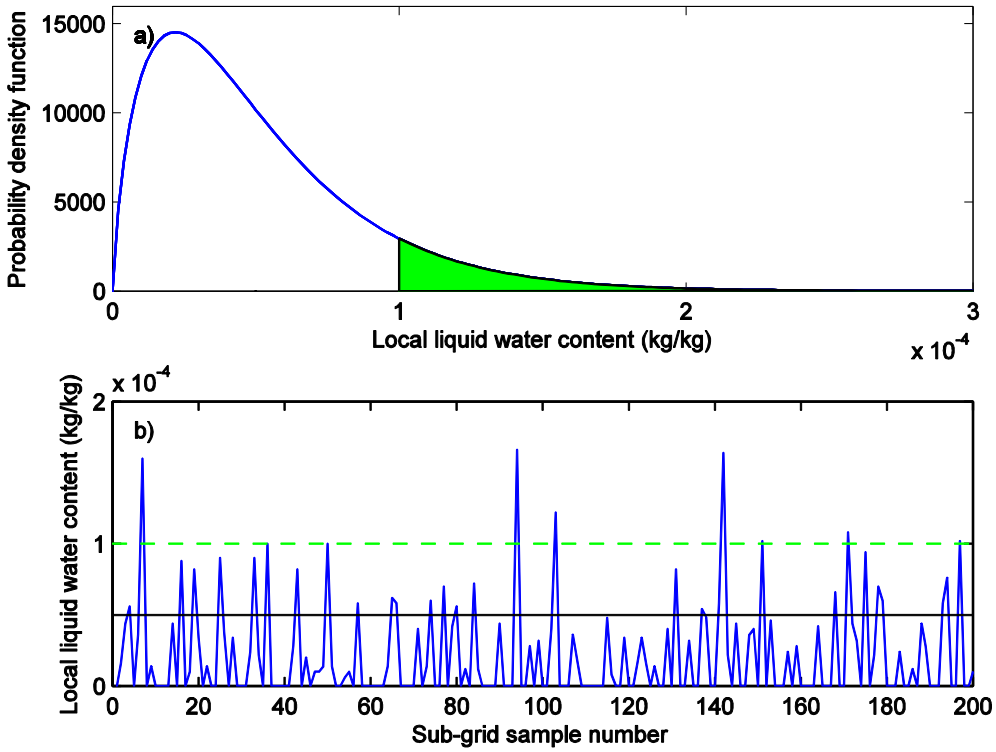

Figure 6: The concept behind the χ icing index. The variability of the local LWC within the cloudy part of the grid-box is represented by an analytical PDF such as the gamma PDF in a), which has a mean value, m = 5.0×10^{-5} kg kg^{-1} and a fractional standard deviation, f_c = 0.75. The threshold LWC is 1.0×10^{-4} kg kg^{-1} and the portion of the PDF where the local LWC is greater than the threshold is shaded. b) Example of variability in local LWC across a model grid-box which has a cloud cover of C_I = 0.5. There are 200 samples, which are randomly determined to be cloudy or clear, and if cloudy their LWC is taken from the PDF.

© Crown copyright 2014

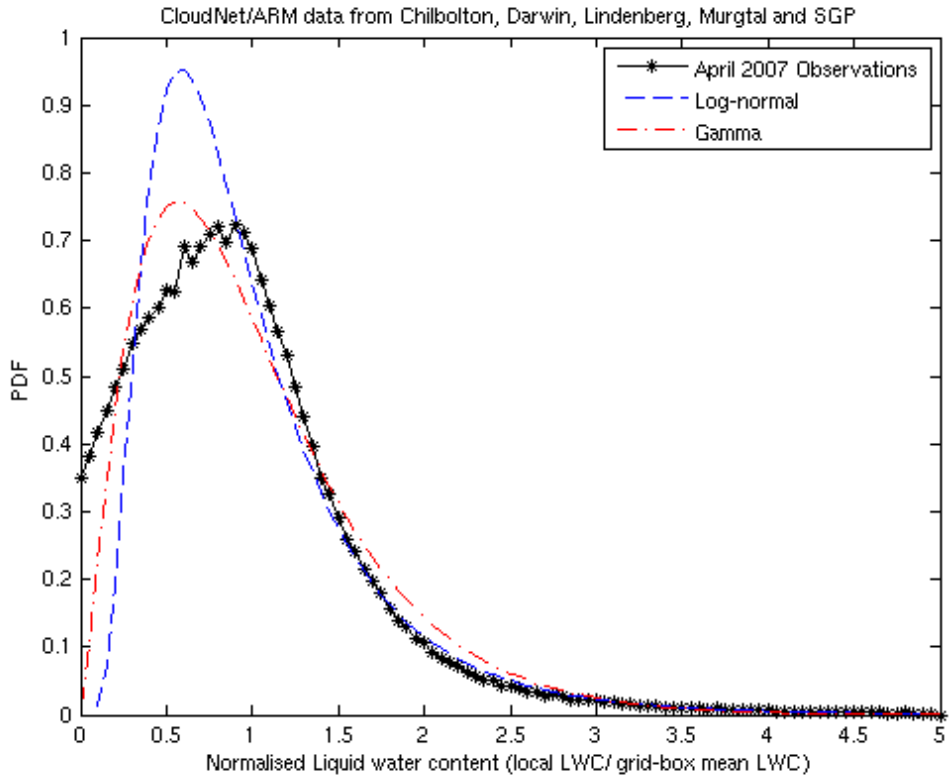

Figure 7: Probability density function (PDF) of liquid water content (LWC) within a grid-box sized region as observed by Cloud-Net and ARM sites during April 2007. The value of local LWC has been normalised by the grid-box mean value to produce a PDF of sub-grid variability which is valid for any grid-box mean value of LWC. The data comes from 5 sites: Chilbolton, Darwin, Lindenberg, Murgtal and Oklahoma. Log-normal and gamma PDF with the same mean (of 1.0) and variance as the observations are plotted for comparison.

© Crown copyright 2014

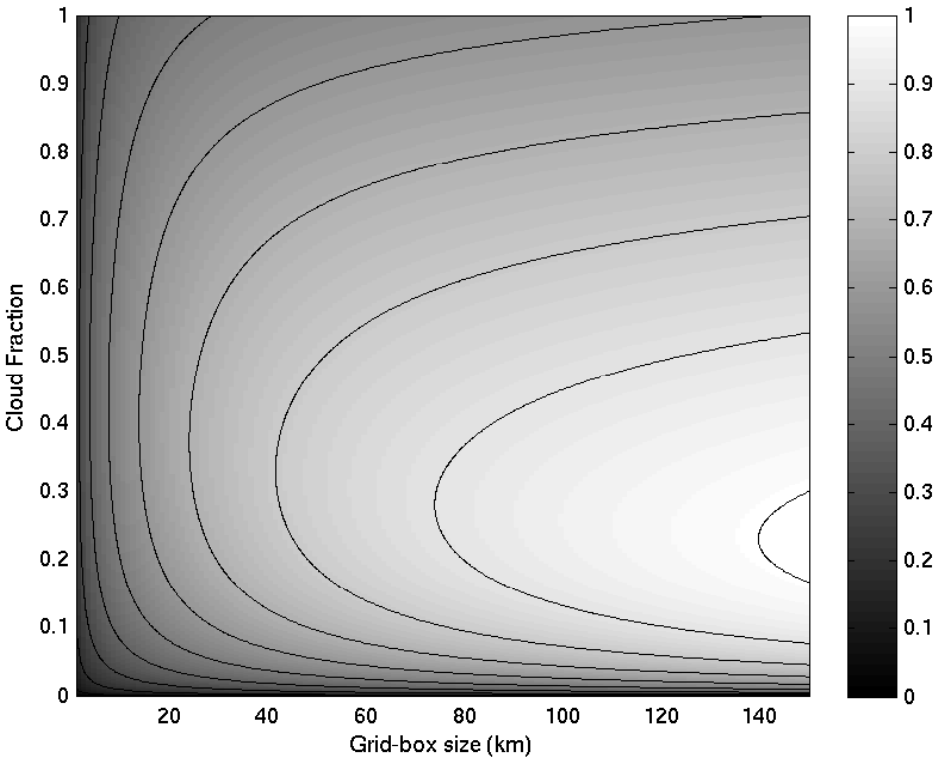

Figure 8: The fractional standard deviation of liquid water content, f_c, as a function of grid-box size and cloud fraction, as given by the Boutle *et al.* (2013) parametrization. Contour intervals every 0.1.

© Crown copyright 2014

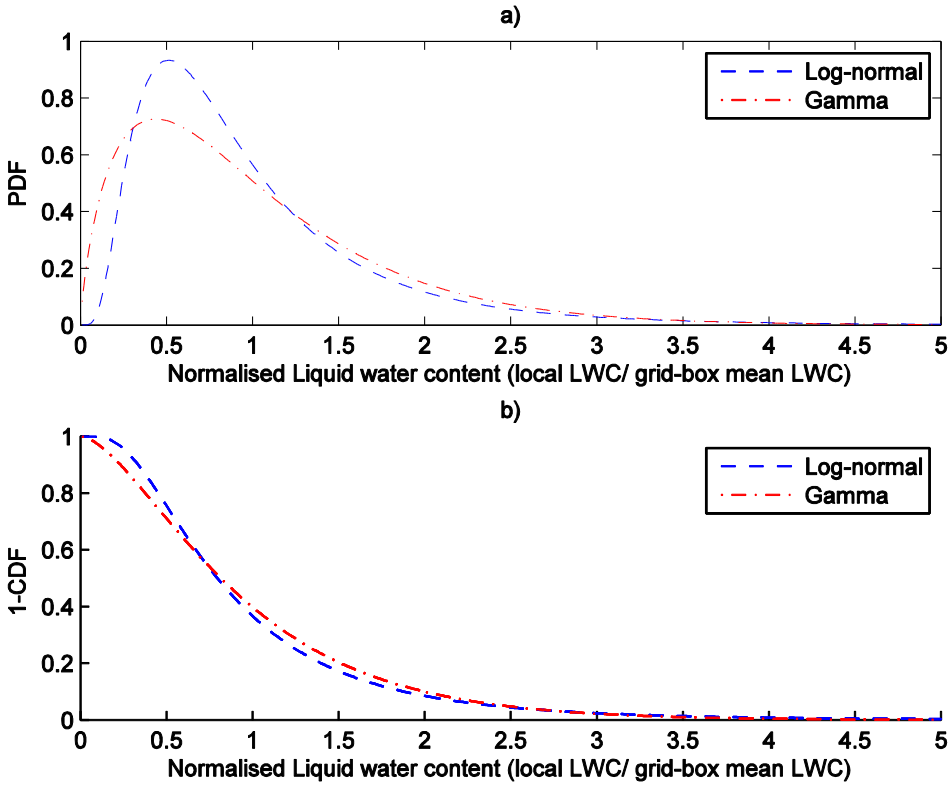

Figure 9: a) A log-normal and a gamma PDF, both with a mean value, m, of 1.0 and fractional standard deviation, f_c, of 0.75. b) The integrals of the log-normal and gamma PDFs to the right of any given point, or 1.0 minus the Cumulative Distribution Function (CDF).

© Crown copyright 2014

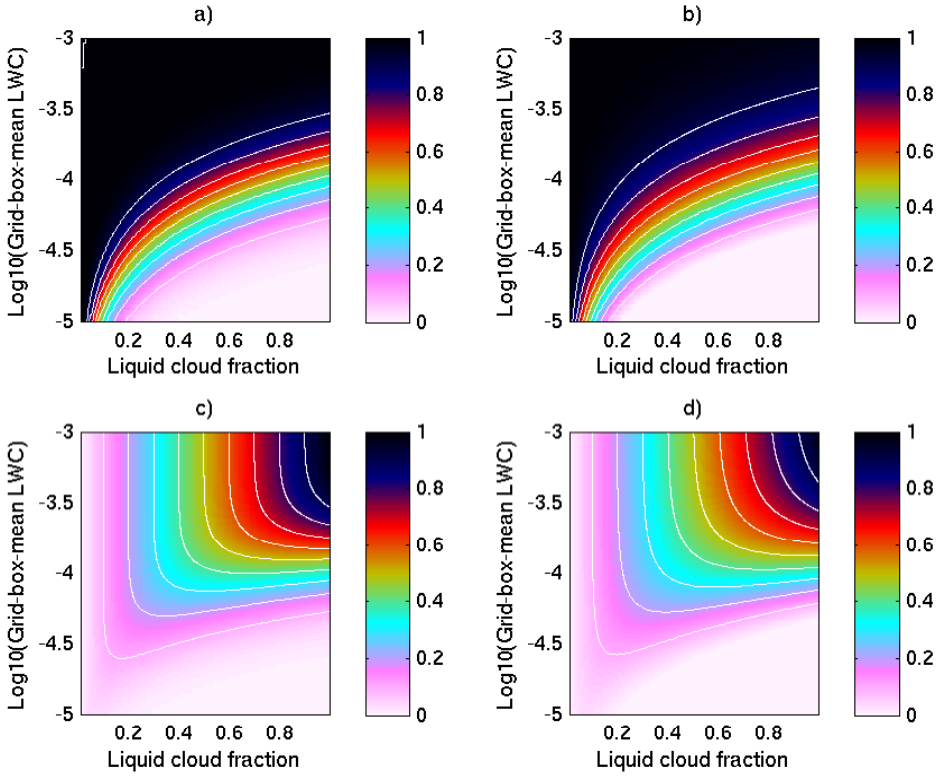

Figure 10: Fraction of cloud (F as defined in Eqn. 16) above threshold, $q_T = 1.0 \times 10^{-4}$ kg kg^{-1}, as a function of liquid cloud fraction and grid-box-mean LWC, a) using a log-normal b) using a gamma PDF. Fraction of sky above threshold (χ as defined in Eqn. 1) as a function of liquid cloud fraction and grid-box-mean LWC, c) using a log-normal d) using a gamma PDF.

© Crown copyright 2014

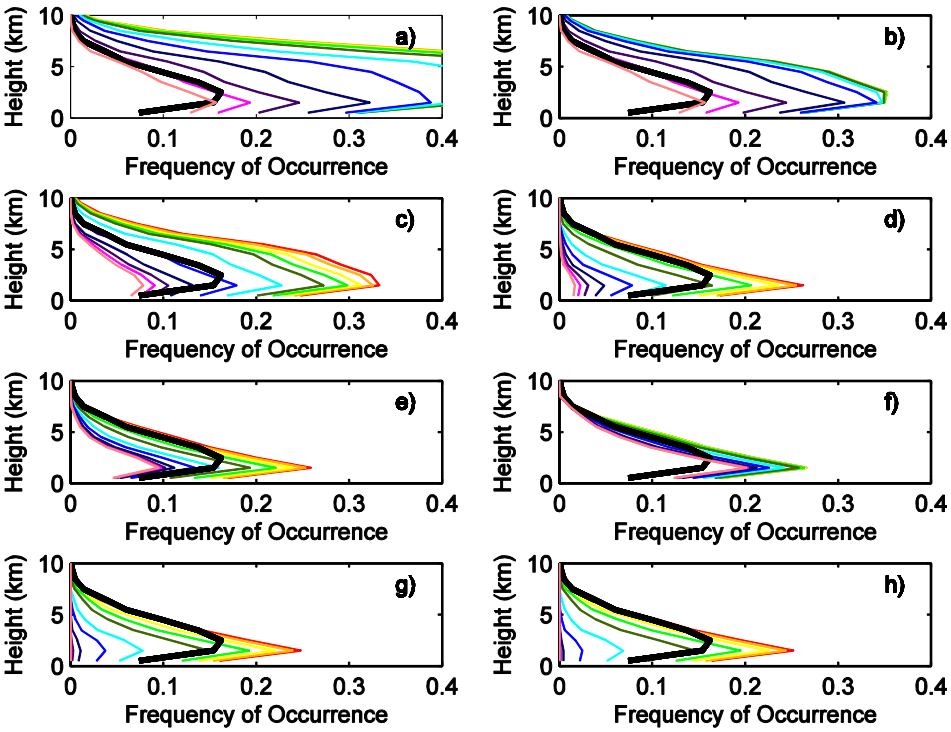

Figure 11: Profiles of model-simulated frequency of occurrence of aircraft icing conditions averaged over the 15 sites world-wide. In each panel the thick black line shows the observations while the coloured lines show the profiles of frequency of icing where icing conditions have been diagnosed by looking for II > ii_{crit} where ii_{crit} =0.01 (red), 0.02 (orange), 0.05 (yellow), 0.1 (light green), 0.2 (dark green), 0.4 (cyan), 0.6 (blue), 0.8 (navy blue), 0.9 (purple), 0.95 (magenta), 0.98 (pink). The different panel correspond to the different icing indices (II) being considered: a) II(RH), b) II(RHCldPres), c) II(CF), d) II(LCF) e) II(LWC), f) II(icLWC) g) II(χ-LN), h) II(χ-Γ).

© Crown copyright 2014

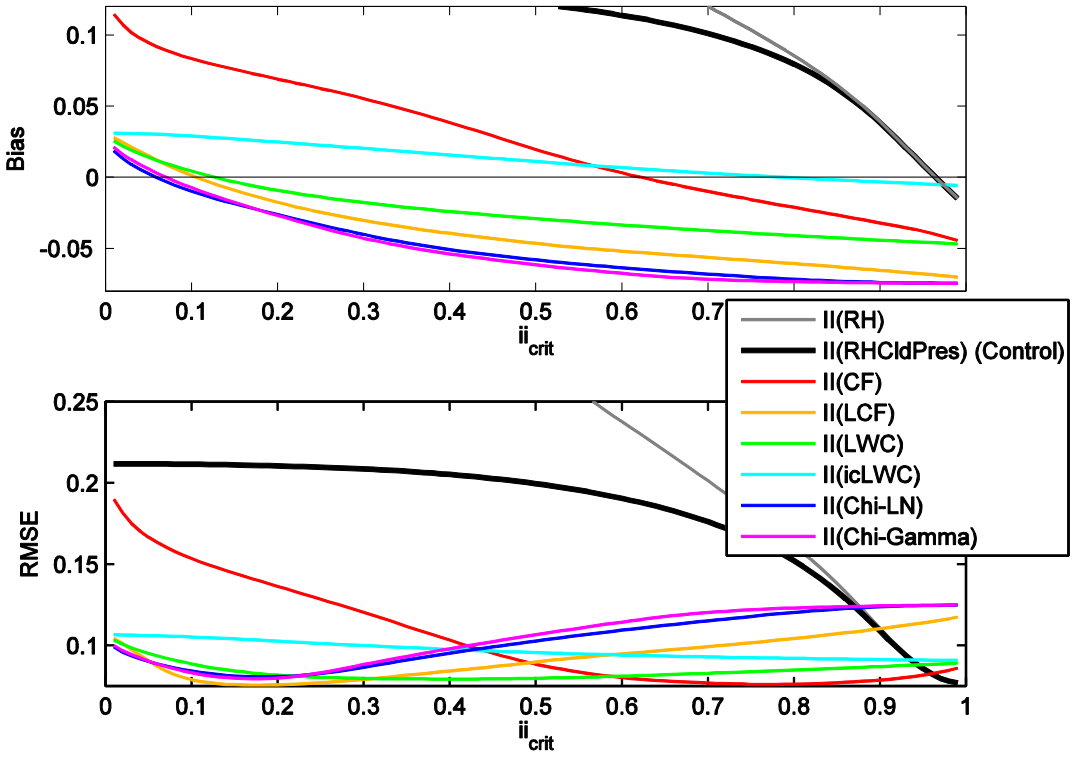

Figure 12: Error in each model-derived icing index (II) as a function of the critical value, ii_{crit}, above which it is assumed that the icing index is predicting icing conditions. The error in the model-derived climatology is quantified by considering the frequency of occurrence at each site, month and height and looking at a) the bias and b) the root-mean squared error, when compared to the observed climatology.

© Crown copyright 2014

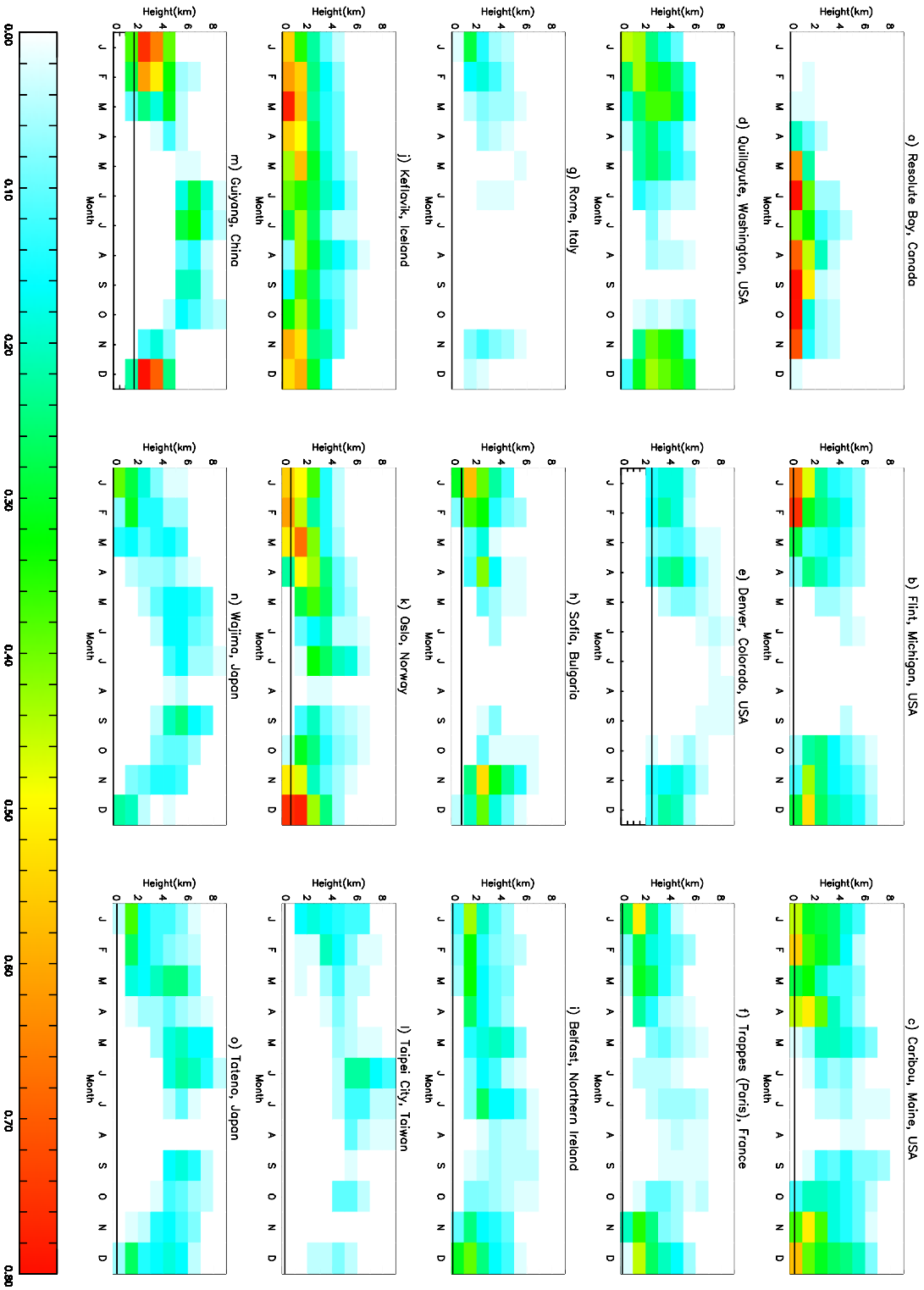

Figure 13: Model-simulated frequency of occurrence of icing conditions at 15 sites world-wide, having defined an icing event as II(RHCldPres)> 0.96.

© Crown copyright 2014

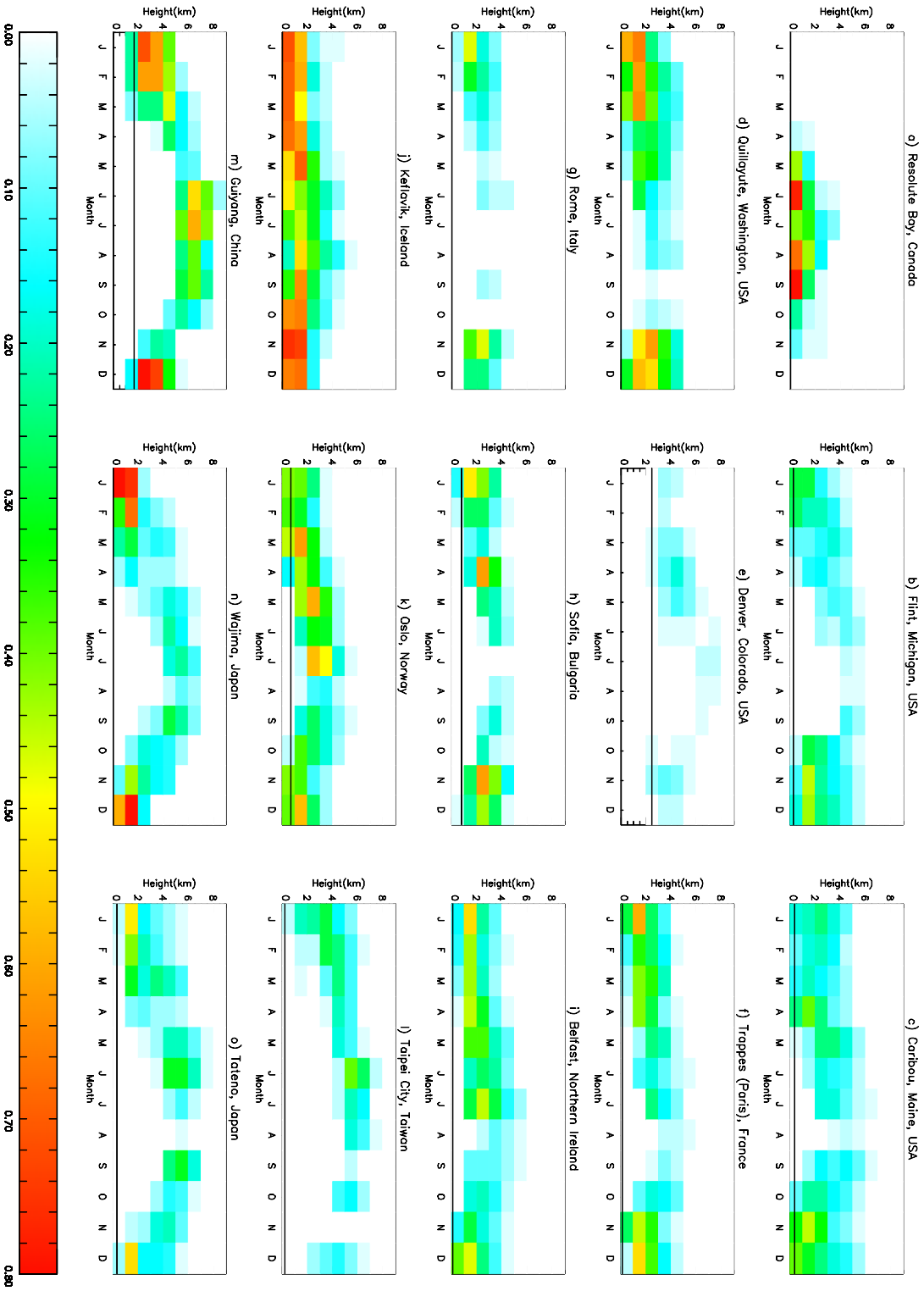

Figure 14: Model-simulated frequency of occurrence of icing conditions at 15 sites world-wide, having defined an icing event as $II(\chi\text{-}\Gamma) > 0.06$.

© Crown copyright 2014

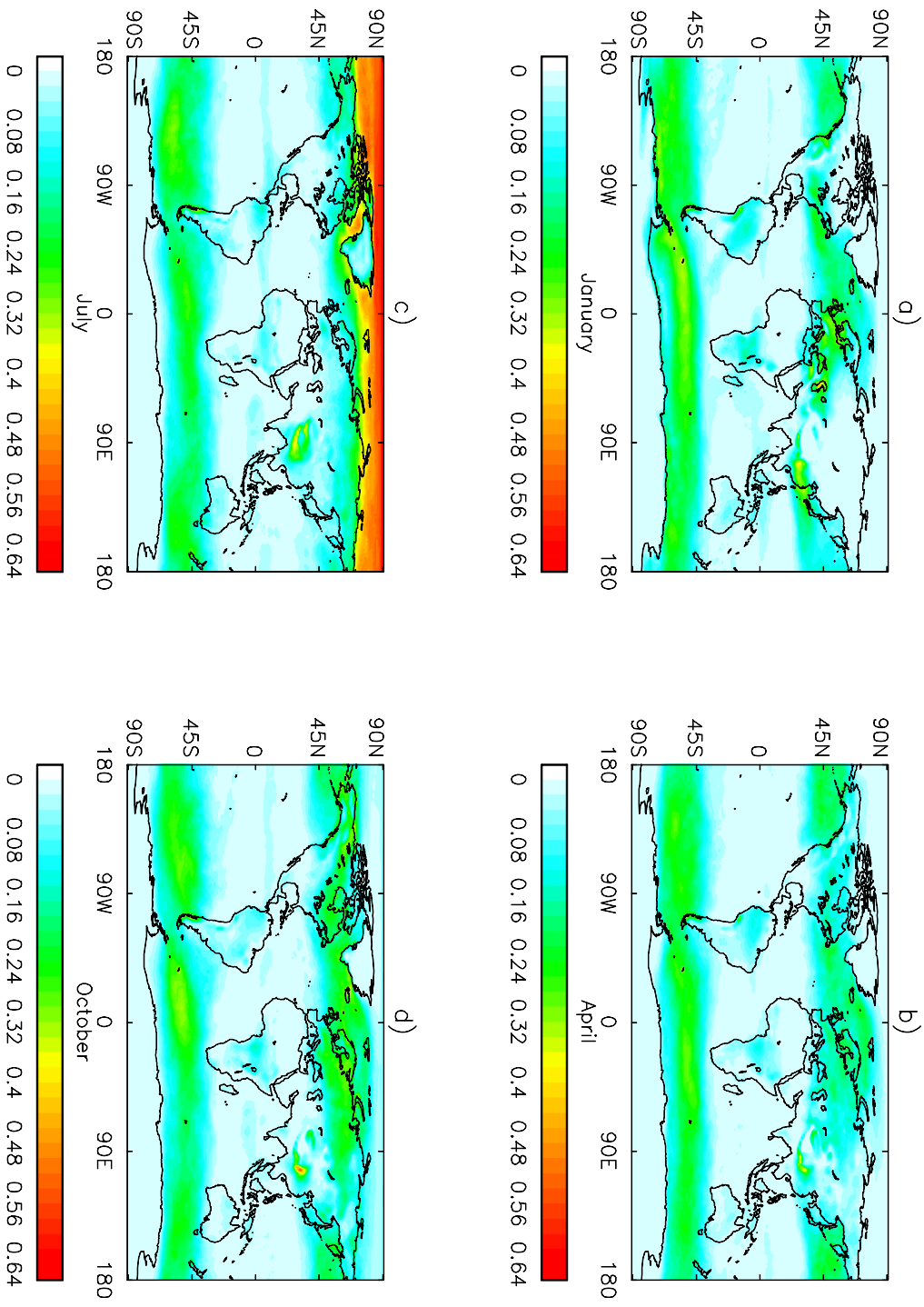

Figure 15: Multi-year mean of total column icing index for the present-day climate for a) January, b) April, c) July and d) October. This is calculated by applying the maximum/random overlap (MRO) algorithm to χ-$\Gamma(1.0 \times 10^{-4})$.

© Crown copyright 2014